2018

Immunologic characteristics of nerves within osteoarthritic marrow regions of human femoral heads

2018

Immunologic characteristics of nerves within osteoarthritic marrow regions of human femoral heads

Rathod, Sonali

BOSTON UNIVERSITY

SCHOOL OF MEDICINE

Thesis

IMMUNOLOGIC CHARACTERISTICS OF NERVES WITHIN OSTEOARTHRITIC MARROW REGIONS OF HUMAN FEMORAL HEADS

by

SONALI RATHOD

B.S., University of California, Davis, 2013

Submitted in partial fulfillment of the

requirements for the degree of

Master of Science

2018

Approved by

First Reader

Louis C. Gerstenfeld, Ph.D.
Professor of Orthopaedic Surgery

Second Reader

Amira I. Hussein Ph.D.
Postdoctoral Fellow

ACKNOWLEDGMENTS

I would like to thank Dr. Louis Gerstenfeld, Dr. Amira Hussein, Dr. Eric Smith, Dr. David Freccero, Dr. Elise Morgan, and Dr. Beth Bragdon, and for guiding me throughout my thesis. I would also like to thank Evan Liu and Anne Hinds for providing fantastic technical support. I thank my fellow students in the Morgan/Gerstenfeld/Bragdon Labs: Joshua Babbin, Matthew Bui, Amanda Molinelli, Jenny Lei, Benjamin Parker, and Meghan Kupraitis.

IMMUNOLOGIC CHARACTERISTICS OF NERVES WITHIN OSTEOARTHRITIC MARROW REGIONS OF HUMAN FEMORAL HEADS

SONALI RATHOD

ABSTRACT

Osteoarthritis (OA) is the most common degenerative joint disease, affecting primarily the hip, knee, and hand (Ip 2005). OA of the knee and hip is the 11th highest contributor to global disability (Cross et al. 2014). Hip OA is diagnosed using radiographs, computed tomography (CT), and/or magnetic resonance imaging (MRI). Hip OA affects the whole hip joint, causing pain and reduced range of motion (Altman et al. 1991). The cause of pain in OA is not well understood, but it may be attributed to abnormal growth of blood vessels and nerves in the subchondral bone of the femoral head (Kumar et al. 2013). Quantifying blood vessels and nerves and correlating their presence with diagnostic techniques such as MRI will establish a relationship between femoral head degeneration and pain levels and current diagnostic signs.

The aims of this study were: (1) to develop a reproducible histological technique to identify blood vessels and nerves in bone sections; and (2) to apply this protocol to identify blood vessel and nerve characteristics within osteoarthritic femoral heads.

Femoral heads were retrieved from 8 OA patients (age range: 40-76; 5 female and 3 male) undergoing total hip replacement surgery. Each sample was evaluated for the presence of subchondral bone cysts using micro-computed tomography (μCT), then regions containing cysts were isolated and dissected for histological processing. Different fixation times in paraformaldehyde (PFA) were tested in three samples to assess the

effect of fixation time on binding of the primary antibody to the target. Samples were stained with hematoxylin and eosin to evaluate overall tissue morphology, safarin-O and fast green to visualize the integrity of articular cartilage, anti-CD31 to identify vascular endothelium, and anti-PGP 9.5 to identify peripheral nerve fibers.

A protocol was successfully developed to identify CD31-positive blood vessels and PGP 9.5-positive nerves in osteoarthritic femoral heads. The immunohistochemistry protocols for staining with anti-CD31 and anti-PGP 9.5 were optimized for maximum intensity of target staining, minimal background staining, and minimal artefactual tissue folding. Fixation time in PFA was not found to have an effect on quality of staining with anti-CD31.

Blood vessels were found in all eight of the samples collected, and peripheral nerves were found in five of the samples. Special attention was paid to regions with fibrous subchondral bone cysts, because these are the most likely type to undergo neurovascular invasion. Out of the five samples with fibrous subchondral bone cysts, blood vessels were identified in all five cyst regions, and peripheral nerves were identified in three cyst regions.

Using the protocols developed in this study, blood vessels and nerves were found in osteoarthritic femoral heads. In future, a larger sample set will be used to correlate the nature of blood vessel density and nerves that are found in bone marrow lesions identified on MRI scans obtained before surgery and are associated with bone cysts. This is an important step towards identifying more effective treatments for OA that address the specific underlying causes and the development of non-treatable pain.

TABLE OF CONTENTS

TITLE……...i

COPYRIGHT PAGE……...ii

READER APPROVAL PAGE……...iii

ACKNOWLEDGMENTS iv

ABSTRACT..... v

TABLE OF CONTENTS..... vii

LIST OF TABLES..... viii

LIST OF FIGURES ix

LIST OF ABBREVIATIONS..... xi

INTRODUCTION 1

METHODS 16

RESULTS 23

DISCUSSION..... 43

CONCLUSION..... 48

REFERENCES 50

CURRICULUM VITAE..... 54

LIST OF TABLES

Table	Title	Page
1	Subjects Enrolled in the Study	16
2	Sample Processing	17
3	PGP 9.5 Staining Trials for Sample 133	22
4	CD31 Staining Trials for Sample 119	23
5	Subject Demographics	25
6	Subject Demographics- Samples Collected Prior to 2017	26
7	Histologically Identified Sclerotic Bone	26
8	Histologically Identified Subchondral Bone Cysts	28
9	Histologically Identified Osteophytes	29
10	PGP 9.5-Positive Nerves	34
11	PGP 9.5-Positive Nerves Within Fibrous Subchondral Bone Cysts	34
12	CD31-Positive Blood Vessels	42
13	CD31-Positive Blood Vessels Within Fibrous Subchondral Bone Cysts	42

LIST OF FIGURES

Figure	Title	Page
1	Compact and Cancellous Bone	4
2	Cartilage Matrix Composition	7
3	Synovial Membrane of the Hip Joint	8
4	Articular Surface of Osteoarthritic Femoral Head	10
5	Method for Cutting Large Sections	18
6	Method for Cutting Small Sections	18
7	Staining Methods Overview	20
8	Sclerotic Bone	27
9	Fibrous Cyst	28
10	Cartilage Intrusion	29
11	Osteophyte	30
12	Sample 133 Region of Interest	31
13	Sample 133 Nerve	32
14	Artefactual Folds in PGP 9.5-Stained Tissue	33
15	The Effect of Amplification on Staining with PGP 9.5	33
16	PGP 9.5-Positive Nerve in a Non-Cyst Region of Sample 111	35

17	PGP 9.5-Positive Nerve in Fibrous Cyst Region of Sample 130	36
18	PGP 9.5-Positive Nerve in a Non-Cyst Region of Sample 131	36
19	PGP 9.5-Positive Nerve in Fibrous Cyst Region of Sample 157	37
20	Blood Vessels Stained with CD31 With and Without Heat Retrieval	38
21	CD31-Positive Blood Vessel in Cyst Region of Sample 152	40
22	CD31-Positive Blood Vessels in Fibrous Cyst Region of Sample 180	40
23	CD31-Positive Blood Vessel in a Non-Cyst Region of Sample 157	41
24	CD31-Positive Vessels in Cyst Region of Sample 119	42

LIST OF ABBREVIATIONS

BMI……Body Mass Index

BP……..Blood Pressure

BSA……Bovine Serum Albumin

CD31……....Cluster of Differentiation 31

CT……Computed Tomography

DAB……..3,3'-Diaminobenzidine

EDTA…….Ethylenediamenetetraacetic acid

H&E…….Hematoxylin and Eosin

HIPAA……...Health Insurance Portability and Accountability Act of 1996

HRP……..Horseradish Peroxidase

HTN……..Hypertension

µCT……..….micro-Computed Tomography

MRI……Magnetic Resonance Imaging

ng…….Nanograms

NIDDM…….Noninsulin Dependent Diabetes Mellitus

NSAID……. Nonsteroidal Anti-Inflammatory Drug

OA……Osteoarthritis

PECAM-1……...Platelet Endothelial Cell Adhesion Molecule

PFA……...Paraformaldehyde

PGP 9.5……..Protein Gene Product 9.5

PPD……Packs Per Day

RANK…… Receptor Activator of Nuclear Factor kappa-B

RANKL……Receptor Activator of Nuclear Factor kappa-B Ligand

THA……Total Hip Arthroplasty

VEGF……Vascular Endothelial Growth Factor

INTRODUCTION

Osteoarthritis Epidemiology

Osteoarthritis (OA) is the most common degenerative joint disease (DJD). Patients with symptomatic OA complain of pain that worsens with weight-bearing activity, morning stiffness, and stiffness after periods of inactivity (Gamble et al. 2000). Hip OA causes reduced range of motion, radiographic joint space narrowing, and subchondral cyst formation or osteophytes (Altman et al. 1991).These structural changes are detectable on x-ray before they cause symptoms, necessitating the distinction between radiographic OA and symptomatic OA (Neogi and Zhang 2013). OA involves degeneration and remodeling of articular cartilage, although it's a whole organ disease and all tissues of the synovial joint- cartilage, subchondral bone, synovium, ligament, capsule, and muscles- participate in the disease progression. OA can affect any synovial joint, but is most common in the knee, hip, and hand (Ip 2005).

OA affects roughly 10% of males and 18% of females over age 60 (Glyn-Jones et al. 2015). Hip and knee osteoarthritis were ranked by the Global Burden of Disease study in 2010 as the 11th highest contributor to global disability (Cross et al. 2014). The Johnston County OA Project found radiographic hip OA to be present in approximately 28% of their cohort of 3000 people age 45 and older. Additionally, it was found that women had a higher prevalence than men, and that African American men had a higher prevalence than Caucasian men (Jordan et al. 2009). There was no difference between African American and Caucasian women (Jordan et al. 2009). Prevalence of hip OA

increases linearly with age (Cross et al. 2014). Thus, an increase in total hip OA cases is anticipated to increase as the population ages.

Primary vs. Secondary OA

Primary OA is due to an idiopathic cause, and is diagnosed by exclusion (Ip 2005). Age is the primary factor predisposing an individual to primary OA. Other major predisposing factors act by changing the load experienced by the hip joint: obesity, abnormal gait, and heavy manual labor (Roach, H and Tilley, S 2007). Ethnicity, genetics, and sex also predispose individuals to primary OA. Females have a higher prevalence and greater severity of OA, though the exact mechanism for the difference between OA progression in women and men has not been elucidated (Neogi and Zhang 2013). Secondary OA develops due to an underlying condition. Diagnoses leading to secondary OA include avascular necrosis (AVN), Paget's disease, inflammatory arthritis, trauma, developmental hip dysplasia (DDH), and Perthes disease (Ip 2005).

Osteoarthritis Treatment

There is no known cure for OA, so treatment for the disease consists of pain management. Physical and occupational therapists provide essential support and guidance for patients with OA. Physical therapists instruct patients on how and when to use heat, exercises, and assistive devices such as canes to relieve discomfort and improve range of motion. Quadriceps strengthening and aerobic exercise are especially important for patients with hip OA (Gamble et al. 2000). Aerobic exercise was found to improve hip

function and decrease pain (Tak et al. 2005). Occupational therapists can help patients protect the hip joint by using medical devices like splints (Gamble et al. 2000). In addition to physical therapy, patients with mild or moderate symptomatic OA may relieve pain by taking nonsteroidal anti-inflammatory drugs (NSAIDs) or acetaminophen. Patients with severe symptomatic OA can be treated with the synthetic opioid agonist Tramadol, or more potent opioid therapy. The American College of Rheumatology recommends pharmacologic therapy only in conjunction with physical and/or occupational therapy (Gamble et al. 2000).

Patients with severe symptomatic OA who have unsuccessfully tried to control their pain with the aforementioned therapies may be candidates for total hip arthroplasty (THA) (Gamble et al. 2000). In 2003, 202,500 THAs were performed in the United States- a number that Kurtz et al. projected to grow to 572,000 by 2030 (Kurtz 2007). 93% of THAs performed in the UK are on patients with the chief complaint of untreatable pain since THA is a cost-effective procedure that yields pain relief and regain of hip joint function (Pivec et al. 2012). Patient selection requires assessing factors including obesity, medical history, and age (Pivec et al. 2012). Patients older than 65 have increased risk of complications. Patients younger than 50 will put more stress on their prosthetic, which will affect the longevity of the replacement (Pivec et al. 2012). The success of this surgical technique, as well as the future of OA treatment, relies on understanding of normal bone and cartilage physiology, as well as the pathophysiology of OA.

Normal Bone Physiology

Bone is a specialized type of connective tissue that provides structural support, protects organs, acts as a reservoir for calcium and phosphate, and produces constituents of blood (Mescher 2016). Bone can be subdivided into compact or cortical bone, and cancellous or trabecular bone (Barrett et al. 2016). The outer portion of long bones such as the femur are composed of compact bone, whereas the interior marrow cavity is composed of trabecular bone (Barrett et al. 2016). Both types of bone are highly vascularized, since blood flow is important for hormone balance, bone remodeling, and repair (Lafage-Proust et al. 2015).

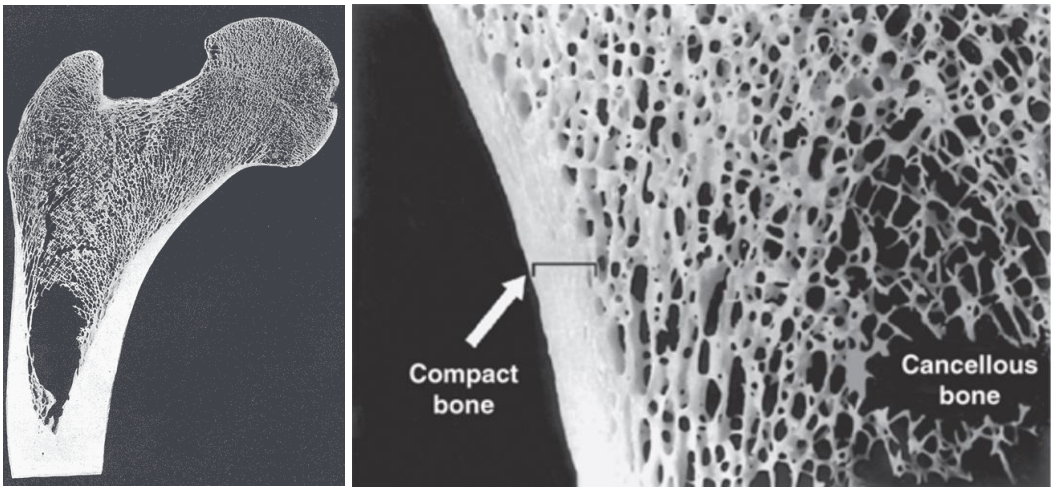

Figure 1: Compact and cancellous bone. Left: Coronal section of the proximal end of the right femur (Gray 1918). Right: 10x photo of the superficial edge of a bone showing the two different structures (Mescher 2016).

Bone, like other types of connective tissue, is composed of cells and extracellular matrix. The principle cell types in bone are osteoblasts, osteoclasts, and osteocytes. Osteoblasts are bone matrix-secreting cells derived from mesenchymal stem cells. As they secrete bone matrix, osteoblasts ultimately surround themselves with it and become

osteocytes (Mescher 2016). Osteocytes are housed in structures called lacunae, and connect with the vasculature through Haversian and Volkmann canals to send and receive nutrients (Barrett et al. 2016). Osteoclasts are large, multi-nucleated cells derived from the monocyte lineage, and function to reabsorb bone. Bone reabsorption occurs in an area sealed off by the osteoclast, called Howship's lacuna. The osteoclast pumps protons into Howship's lacuna, thereby acidifying and eroding the hydroxyapatite crystals of the bone extracellular matrix (ECM). Proteases are also released into Howship's lacuna, which degrade collagen. The degraded ECM is transcytosed across the osteoclast and released into the interstitial space.

Bone remodeling is a constant process involving all three of these cells acting synergistically (Mescher 2016), and is under both local paracrine and systemic hormonal control (Barrett et al. 2016). Osteoblasts express receptor activator for nuclear factor kappa-B ligand (RANKL) on their cell surface- the ligand for receptor activator for nuclear factor kappa-B (RANK) expressed on the surface of monocytes. When RANKL activates RANK, monocytes differentiate into osteoclasts (Barrett et al. 2016). After osteoclasts break down bone, osteoblasts rebuild bone in the spaces left behind (Barrett et al. 2016).

Bone matrix contains hydroxyapatite crystals composed of calcium phosphate, as well as type I collagen, proteoglycans, and glycoproteins (Mescher 2016). 99% of the body's calcium is stored in bone. Calcium is an important ion for muscle contraction and nerve function, among many other things. Parathyroid Hormone (PTH) acts directly on bone to increase bone resorption and therefore increase Calcium concentration in the

blood. Calcitonin, produced by the thyroid, directly inhibits bone resorption by acting on osteoclasts, therefore decreasing blood calcium levels (Barrett et al. 2016). Because 90% of the organic matter is type I collagen, bone tissue is acidophilic after decalcification.

Bone remodeling is important not only for mineral metabolism, but for bone repair and maintenance of skeletal strength. Fracture repair requires bone remodeling to reshape the bone callus forming in the fracture gap. Blood released from vessels broken during fracture forms a clot. The clot is gradually broken down by macrophages, and a fibrocartilaginous procallus forms. The procallus is invaded by new blood vessels and osteoblasts. A hard callous is formed by osteoblasts depositing woven bone- a loosely organized type of bone. This bone will be remodeled by osteoclasts and osteoblasts into compact or trabecular bone, at which point the original morphology is restored (Mescher 2016).

Normal Cartilage Physiology

Cartilage, like bone, is a special type of connective tissue. Articular cartilage can act to absorb impact because of its extracellular matrix (Roach, H and Tilley, S 2007). 70-80% of cartilage is water. 15% is collagen, of which type II is most prevalent. Type II collagen creates an underlying fibrous scaffold, which holds proteoglycan molecules into place and imparts incompressible strength (Figure 2). Aggrecan accounts for 9% of cartilage. Proteoglycans are composed of hyaluronic acid and chondroitin sulfate interacting with aggrecan. They are highly hydrophilic due to their large number of fixed negative charges and will bind large volumes of water, thus providing the main

compressor physical property to the cartilage tissue. When cartilage is compressed, water is pushed away briefly, but the proteoglycans draw water back to it quickly causing the cartilage matrix to regain its original shape (Aigner and Stove, J 2003). While chondrocytes, the resident cells of cartilage, are important for creating the extracellular matrix, they do not directly provide structural support or elasticity for the tissue (Felson 2015).

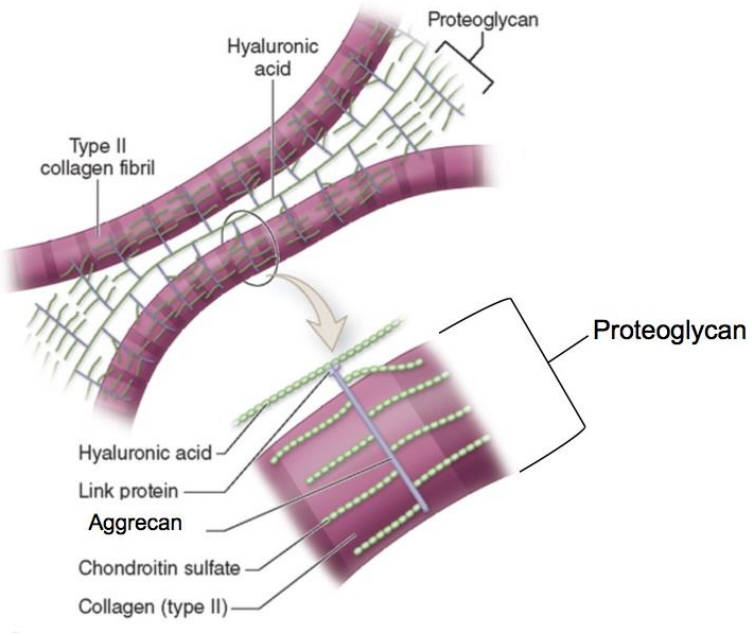

Figure 2: Cartilage Matrix Composition. Type II collagen fibrils with proteoglycans interspersed (modified from Mescher 2013).

Healthy articular cartilage is resistant to vascularization and is aneural (Sunita Suri and Walsh 2012). Chondrocytes receive nutrients and excrete waste into the water of the ECM, and blood vessels usually exist only in the synovium and subchondral bone (Sunita Suri and Walsh 2012).

The Hip Joint

The ball-and-socket structure of the hip, or femoroacetabular, joint reflects its function as the major weight-bearing joint in the human body. The acetabulum of the pelvis articulates inferior/mediolaterally with the femoral head. The articular cartilage, bones of the femur and hip, ligaments, and muscles crossing the hip joint impart stability. The muscles of the hip joint are the strongest in the body (Feeko and Mallow 2015).

The hip joint is a synovial joint, and thus has a synovium composed of adipose tissue, fibroblasts, and macrophages. Synovial fibroblasts secrete synovial fluid, which serves as a joint protector along with the stabilizing structures of the hip. Synovial fluid reduces friction between articular cartilage of the acetabulum and femoral head, and is composed of hyaluronic acid and glycoproteins (Felson 2015).

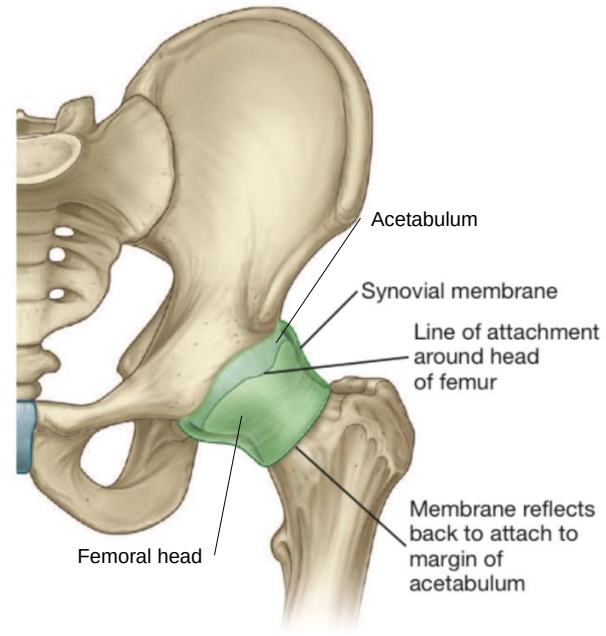

Figure 3: Synovial Membrane of the Hip Joint. Synovial membrane is shown in green (modified from Drake, Vogl, and Mitchell 2012).

Osteoarthritis Pathology

Cartilage Degeneration

Early in the disease progression, articular cartilage of the affected joint becomes irregular due to uneven cartilage loss (Felson 2015). The role of cartilage as a shock-absorber is compromised as it wears down, which propagates further damage (Roach, H and Tilley, S 2007). Chondrocytes in the damaged area undergo mitosis, producing clusters of cells similar to those seen in the proliferative zone of endochondral ossification. This causes a local decrease in proteoglycan concentration, and subsequent decrease in cartilage elasticity and strength (Felson 2015).

In contrast to healthy cartilage, OA cartilage is prone to vascular invasion from subchondral bone. Loss of proteoglycans and expression of vascular endothelial growth factor (VEGF) by chondrocytes are two mechanisms that have been observed to contribute to vascularization of OA cartilage (Sunita Suri and Walsh 2012). Clinically, cartilage loss is assessed radiographically and it presents as joint space narrowing on radiographs (Felson 2015).

Osteophytes

Osteophytes are bony outgrowths that form in the non-weight bearing regions of the femoral head after the cartilage has degenerated (Roach, H and Tilley, S 2007). They form from projections of cartilage that ossify instead of re-covering the area of cartilage

damage (Felson 2015). Osteophytes can be small or large, and can restrict joint movement and cause pain (Roach, H and Tilley, S 2007).

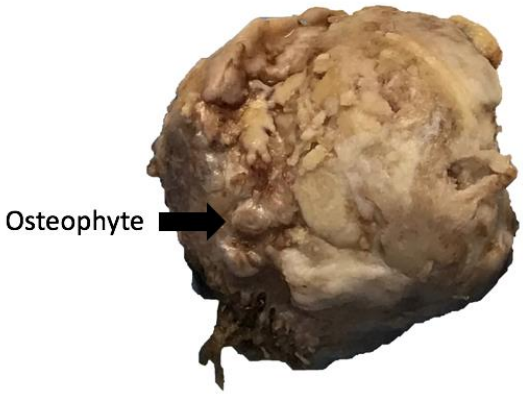

Figure 4: Articular Surface of Osteoarthritic Femoral Head. Cartilage degeneration and osteophytes are visible in this image of Sample 157.

Subchondral Cysts

As articular cartilage degenerates, cytokines signal activation of osteoclasts and osteoblasts to remodel the subchondral bone (Felson 2015). Cartilage in the weight-bearing region of the femoral head articular surface is the first to degenerate (Roach, H and Tilley, S 2007). Within these regions bone is lost with the formation of structures termed *subchondral cysts*. These areas of bone loss occur more frequently in subchondral trabecular bone since these areas remodel significantly more than deep trabecular bone (Li et al. 2015). Because of the differences between male and female bone density, it was hypothesized that males and females would have different bone remodeling parameters, but Li et al. found that there was no significant difference (Li et al. 2015). This finding could be due to analysis of osteoarthritic femoral heads only- no age-matched healthy femoral heads were analyzed (Li et al. 2015).

Two competing theories exist for the formation of subchondral bone cysts in OA: the "fluid breach theory" and the "bony contusion theory". The fluid breach theory posits that cyst formation is initiated by synovial fluid leaking through cracks in the articular cartilage into the subchondral bone (Landells 1953). The bony contusion theory states that bone that is overloaded or incorrectly loaded dies and is liquefied and subsequently removed by osteoclasts, creating a cyst. This theory is supported by a 2015 study by Chen et al., where subchondral cysts from subjects with knee OA were analyzed using micro computed tomography (μCT) and histology. The finding that trabeculae surrounding cysts had a stiffer microarchitecture and higher BMD, combined with confirmation of increased osteoblast and osteoclast activity, suggested to the authors that the bony contusion theory is more accurate than the fluid breach theory (Chen et al. 2015).

Subchondral Bone Sclerosis

Bone sclerosis is a hallmark of OA, and is simply an increase in bone density caused by increased bone turnover and prolonged period of tissue mineralization (Hügle and Geurts 2016). Klose-Jensen et al. found that in human OA, increased bone turnover occurs before subchondral bone sclerosis. They also found that bone volume was maximum in the area of most severe cartilage degradation, but bone turnover increases in other regions underlying lesser cartilage degradation. These findings indicate that OA is caused by excessive bone formation in all areas of the femoral head, including outside the weight bearing region (Klose-Jensen et al. 2015).

Detection of OA

Clinical Findings & X-Ray

The American College of Rheumatology identifies important clinical criteria for correctly classifying DJD as OA. They are: reduced internal rotation or internal rotation with pain, hip stiffness in the morning, and advanced age. OA patients develop symptoms gradually, often beginning with stiffness and progressing to pain during motion that is relieved by rest (Hellmann and Imboden Jr. 2017). Mild, but not severe, inflammation of the affected joint is possible (Hellmann and Imboden Jr. 2017). The observations of osteophytes and joint cavity narrowing in radiographs, along with clinical findings, confirm hip OA (Altman et al. 1991).

MRI Lesions

Magnetic Resonance Imaging (MRI) is useful as a diagnostic tool because, unlike x-ray, it can differentiate between bone, cartilage, and soft tissue (Roemer et al. 2009). OA associated Bone Marrow Lesions (BMLs) are ill-defined regions directly underneath damaged articular cartilage. They may be present anywhere in the subchondral bone of the joint affected by OA. BML volume has been found to be directly proportional to the extent of cartilage loss and radiographic joint space narrowing (Roemer et al. 2009). MRI is useful in discriminating OA from other diseases that cannot be detected using clinical signs and x-ray, like transient osteoporosis (Roach, H and Tilley, S 2007). The exact

histological nature of MRI lesions to structural loss and tissue composition has not been well defined.

Relationship of Nerves and Blood Vessels in the Development of OA

Cluster of Differentiation 31 (CD31) is a marker used for detecting the endothelium of blood vessels. In humans, marrow sinusoids, marrow arterioles, and capillaries are CD31-positive (Lafage-Proust et al. 2015). In 2016, Shabestari et al. used CD31 as a tool for histologically identifying the extent of vascularity in MRI-identified BMLs in subjects with hip OA. They found that BMLs had significantly greater vascularity, and that angiogenesis occurred in these regions (Shabestari et al. 2016). Vascular invasion of subchondral bone in a rabbit model of knee OA was studied by Saito et al. in 2012. The conclusion was that increased angiogenesis of the osteochondral junction preceeded increased vascular invasion, and that both processes are features of early OA (Saito et al. 2012). These findings suggest that samples taken from subjects with late-stage hip OA should have an increased number of blood vessels, and that they will be CD31-positive.

Protein Gene Product 9.5 (PGP 9.5) is a peripheral nerve marker that has been used in several recent studies assessing potential causes of pain in musculoskeletal disease. Cher et al. used PGP 9.5 to visualize nerves in the shoulder capsule of subjects with frozen shoulder- a common musculoskeletal disability. The hypothesis that nerve fiber density would be increased in affected samples was upheld (Cher et al. 2017). Netzer et al.'s 2016 study of lumbar facet joint OA found PGP 9.5 positive nerve fibers in

bone samples from affected subjects, though they were not exclusively present in areas of pathological bone structure. This study found that PGP 9.5 positive nerve fibers were closely associated with blood vessels (Netzer et al. 2016). Suri et al. successfully used PGP 9.5 to visualize nerves in articular cartilage near the osteochondral junction and the bone marrow cavity of osteophytes from tibial plateaus of subjects with tibiofemoral OA. The nerve fibers were near blood vessels in these two locations. Free nerve fibers were found in subchondral bone marrow. From these observations, it was concluded that nerves grow into articular cartilage and osteophytes from subchondral bone (S. Suri et al. 2007).

Objectives

Osteoarthritis is the most prevalent degenerative joint disease, and it is projected to affect an increasing number of people due to the aging population. Treatment options are currently limited, and though total hip arthroplasty is effective, it is only performed once patients have advanced hip OA. Understanding the underlying biological mechanisms that lead to the progression of OA and development of chronic pain is a crucial step in identifying more effective treatments that treat the specific underlying causes of OA and the development of non-treatable pain.

The aims of this study were: (1) to develop a reproducible histological technique to identify blood vessels and nerve in bone sections; and (2) to apply this protocol to identify blood vessel and nerve characteristics within osteoarthritic femoral heads.

In future, a larger sample set will be used to correlate the nature of blood vessel density and nerves that are found in bone marrow lesions identified on MRI scans obtained before surgery and are associated with bone cysts. This is an important step towards identifying more effective treatments for OA that address the specific underlying causes and the development of non-treatable pain.

METHODS

Femoral Head Collection

Femoral heads were collected from subjects (n=3; age range: 40-58; sex: 2 female and 1 male; side: 2 right and 1 left) undergoing total hip arthroplasty as a treatment for late stage OA at Boston Medical Center in 2017. Subjects were consented according to HIPAA guidelines prior to the surgery and were offered a copy of the consent form. Subjects were male and female, and were between the ages of 40 and 58 years old. Samples were collected from either side of the body. Samples collected prior to 2017 (n=5; age range: 45-76; sex: 3 female and 2 male; side: 1 right and 4 left) were also used in this study, and were collected and processed in the same way (Table 1).

Table 1. Subjects Enrolled in the Study

Subject #	Sex	Age	Side
111	M	70	Left
119	F	72	Left
130	F	55	Left
131	F	76	Left
133	M	45	Right
152	F	40	Right
157	M	58	Right
180	F	50	Left

Samples were placed into phosphate-buffered saline (PBS) with 1% penicillin/streptomycin immediately upon collection from the operating room. Within 30

minutes of each surgery, the neck was separated from the head using a reciprocating saw (Dremel, WI), and the head was placed into 4% paraformaldehyde at 4ºC. To maintain tissue integrity for imaging and histology, samples were fixed in paraformaldehyde (PFA). Different fixation times were tested in three samples to assess the effect of fixation time on binding of the primary antibody to the target. Each sample was processed differently, according to table 2. Samples collected prior to 2017 were all in PFA for two weeks. After fixation in PFA, samples were placed into 1x PBS with 1% penicillin/streptomycin to await μCT scanning.

Table 2. Sample Processing

Sample #	Time in PFA at 4ºC
152	2 weeks
157	1 week
180	0 weeks

Femoral Head Sectioning

Samples were scanned using a Zeiss Xradia μCT (Zeiss, Germany) to identify cyst regions then sectioned with an IsoMet 4000 brand low-speed abrasive rotating blade (IsoMet, VA) (Figure 5). Each section was numbered, photographed, and stored in 1x PBS with 1% penicillin/streptomycin.

The samples were cut into smaller pieces to eventually fit onto a 75mm by 25mm microscope slide with the Dremel reciprocating saw (Figure 6). The samples were then placed into PFA for a second time to complete the fixation process. Sample 152 and Sample 157 were in PFA for one week, and Sample 180 was in PFA for two days.

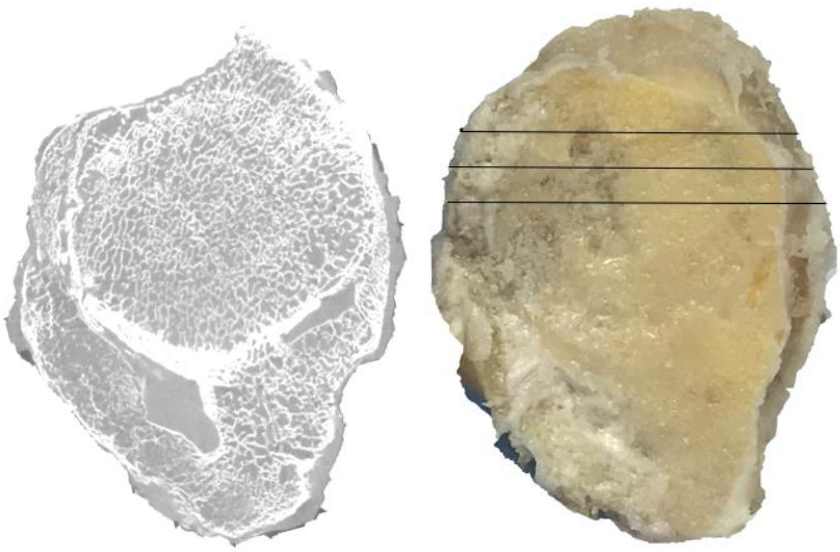

Figure 5: Method for cutting large sections. Left: µCT image of Sample 152 in anatomical position; Right: Sample 152 prior to being cut with the IsoMet 4000, with black lines indicating where cuts will be made

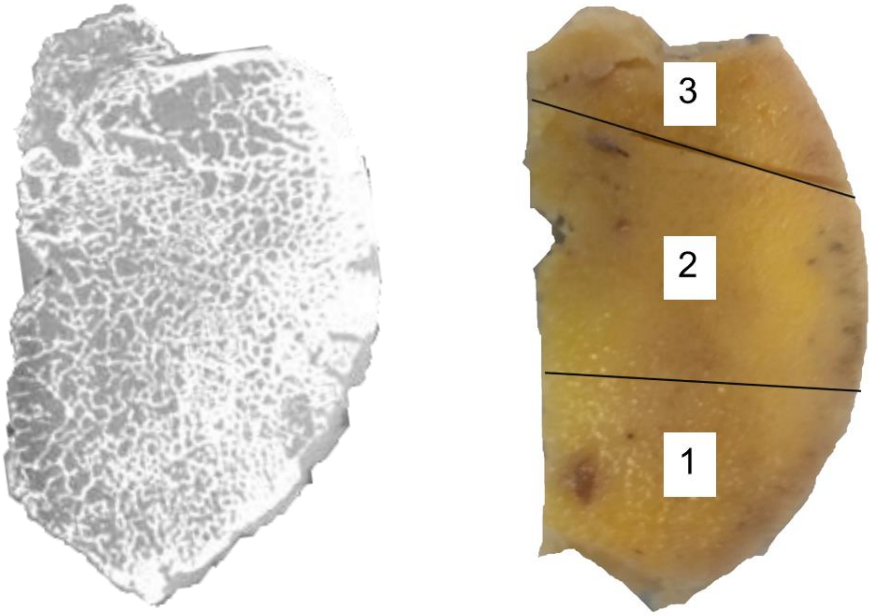

Figure 6: Method for cutting small sections. Left: µCT image of Sample 152 showing regions of varying bone density and orientation of trabeculae; Right: Picture of Sample 152A prior to being cut with the Dremel, with black lines indicating where cuts will be made

Decalcification

Following PFA, the samples were washed with 1x PBS for approximately 1 hour to remove residual PFA on the tissue surface. They were then decalcified in 14% Ethylenediamenetetraacetic acid (EDTA) for three weeks. Each sample was placed in a nylon mesh biopsy bag containing an index card with the sample number written on it in pencil, then all samples were put into a large container in the cold room at 4ºC on a rocking shaker. EDTA was changed every 3-4 days.

After three weeks, samples were tested with a 30-gauge needle to check for consistency. Samples that were soft, with a tofu-like consistency, were x-rayed to confirm that they were completely decalcified. Samples that were not found to have opaque regions of calcified bone were then fixed in 4% PFA for a third time overnight, washed in PBS for 30 minutes, and placed in 70% Ethanol.

Histology

Samples were embedded in paraffin, and 15x 5µm thick slices were mounted on slides. Each slide was inspected for artefact, and the slides with the fewest artefacts were prioritized for staining. Two serial slides were selected and stained with Hematoxylin & Eosin (H&E) to visualize overall tissue morphology, and Safarin-O/Fast Green to visualize cartilage. A third slide was stained with PGP 9.5 (Sigma-Aldrich Product #SAB4503057) to visualize peripheral nerve, and a fourth slide was stained with an antibody to CD31 (Invitrogen Product #PA5-29166**)**.

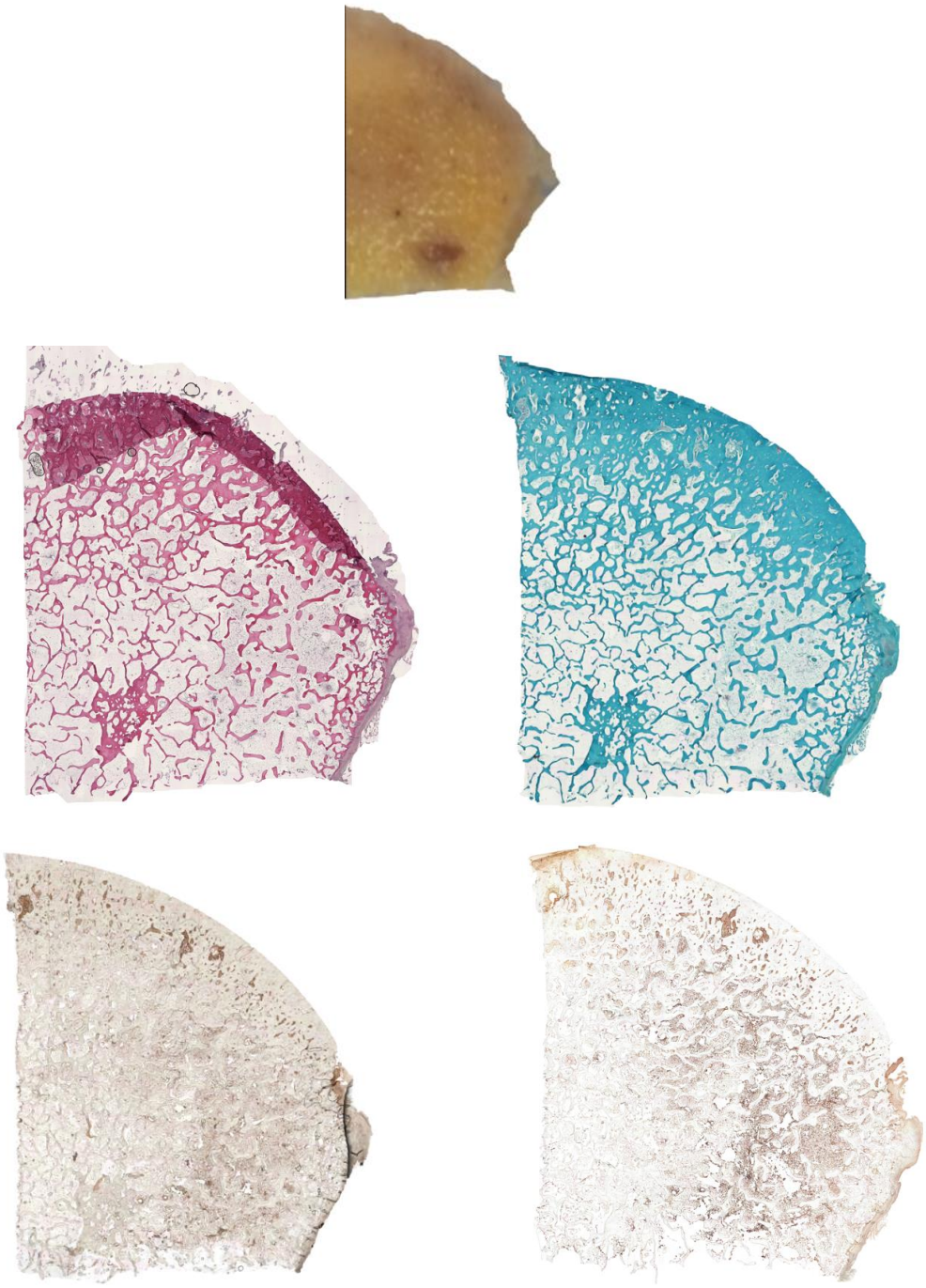

Figure 7: Staining Methods Overview. Top center: Photo of Sample 152A1 before decalcification; Middle left: Histological section of Sample 152A1 stained with H&E; Middle right: Histological section of Sample 152A1 stained with Safarin-O/Fast Green; Bottom left: Histological section of Sample 152A1 stained with an antibody to PGP9.5; Bottom right: Histological section of Sample 152A1 stained with an antibody to CD31

The different staining techniques allowed for identification of several important features. Samples were scanned for the presence of sclerotic bone, osteophytes, and subchondral bone cysts. The subchondral bone cysts were further classified using visualization with H&E and Saf-O.

Immunohistochemistry

Slides to be stained with PGP 9.5 were first deparaffinized in xylene and ethanol. The samples were then either heat-retrieved, or not. Heat retrieval was performed by placing slides in a tray containing antigen unmasking solution (Vector, PA). The samples were microwaved for five minutes on power four, then five minutes on power three, and finally for five minutes on power three again. Samples were allowed to cool slightly before continuing to the blocking steps.

Both heat-retrieved and non-heat-retrieved samples were then treated with a hydrogen peroxide block (abcam) for ten minutes, washed with 1x PBS, and treated with a protein block (abcam) for 10 minutes. After washing again with 1x PBS, treated with the primary antibody. The primary antibody used was anti-PGP 9.5 (Sigma Aldrich) diluted 1:50, 1:100, or 1:500 with 1x PBS and 1% BSA. Samples were incubated overnight at 4ºC. The following day, samples were washed with 1x PBS, then treated with HRP-conjugate (abcam) for 15 minutes. Samples were washed again, then in some samples the target was amplified.

For amplification, samples were treated with biotin tyramide (Perkin Elmer) for 10 minutes at room temperature. Samples were then washed with 1xPBS, and treated with streptavidin-HRP (Perkin Elmer) for 30 minutes at room temperature.

After washing with 1xPBS, both amplified and non-amplified samples were treated with DAB chromogen/DAB substrate (abcam) for 8 minutes at room temperature. The samples were then either counterstained with Hematoxylin by dipping once, or not. A coverslip was applied using EcoMount mounting medium (BioCare Medical).

This procedure was optimized using Sample 133, which was collected prior to 2017.

Table 3. PGP 9.5 Staining Trials for Sample 133

Slide ID	Concentration	Hematoxylin	Heat Retrieval	Amplification
A	1:50	+	-	-
B	1:100	+	-	-
C	1:500	+	-	-
D	1:50	+	+	-
E	1:100	+	+	-
F	1:500	+	+	-
G	1:100	-	-	+
H	1:100	-	-	-

The staining protocol for CD31 was the same as the staining protocol for PGP 9.5, but fewer trials were done to find the optimal staining method. Sample 119, another sample collected prior to 2017, was used for this experiment.

Table 4. CD31 Staining Trials for Sample 119				
Slide ID	Concentration	Hematoxylin	Heat Retrieval	Amplification
A	1:100	-	-	+
B	1:100	-	+	+

RESULTS

Subject Demographics

Femoral heads were collected from subjects (n=3; age range: 40-58; sex: 2 female and 1 male; side: 2 right and 1 left) undergoing total hip arthroplasty as a treatment for late stage OA at Boston Medical Center in 2017 (Table 5). Samples collected prior to 2017 (n=5; age range: 45-76; sex: 3 female and 2 male; side: 1 right and 4 left) were also used in this study (Table 6).

Sclerotic Bone

Identifying sclerotic bone was important because sclerotic bone is found around subchondral cysts in OA (Glyn-Jones et al. 2015). Trabecular bone with increased density was identified as sclerotic bone. Figure 8 shows several samples that were positive for subchondral bone sclerosis. All eight samples had sclerotic bone (Table 7).

Subchondral Bone Cysts

Each sample was surveyed for the presence of subchondral bone cysts in the region that was processed for histology. Cysts are regions where the normal trabecular bone and marrow are displaced by another tissue type. Cysts were identified as fibrous, fatty, or as having a cartilage intrusion. These respective categories identify the tissue that pathologically replaces subchondral bone during the disease progression of OA. Sample 180 did not have a cyst.

Table 5. Subject Demographics.			
Subject #	152	157	180
Sex	F	M	F
Age	40	58	50
Side	Right	Right	Left
Race	N/A	White	White
BMI [kg/m^2]	32.6	29.71	27.4
Height [cm]	163	176	163
Weight [kg]	86.2	92	72.4
Diabetes	No	No	No
Renal Disease	No	No	No
History of steroid use	No	No	No
Alcohol abuse	No	Yes	Former
Smoking status	No	0.25PPD	Former
Vitamin D level [ng/mL]	N/A	22.2	34.1
Hemoglobin A1C	5.1	5.8	5.1
Cardiovascular disease	No	No	No
Sickle cell	No	No	No
BP (systolic/diastolic)	130/78	112/72	123/72
Heart rate	101	89	84
Multiple limb OA	No	Yes	No
HTN	No	Yes	No
Hyperlipidemia	No	No	Yes
Osteoporosis	No	No	No
Osteonecrosis	No	Yes	No
Low bone mass	No	No	No
Diagnosis if ≤40 y/o	Primary diagnosis OA, Secondary diagnosis Smith Magenis syndrome		

Table 6. Subject Demographics- Samples collected prior to 2017					
Subject #	111	119	130	131	133
Sex	M	F	F	F	M
Age	70	72	55	76	45
Side	Left	Left	Left	Left	Right
Race	White	African American	African American	White	White
BMI [kg/m2]	39.1	28	28.6	33.6	29.5
Weight [kg]	115	N/A	87.9	83.3	100.9
Diabetes	No	DM	No	No	No
Renal Disease	No	Renal Insufficiency	No	No	No
History of steroid use	No	No	No	No	No
Alcohol Abuse	No	No	No	No	No
Smoking Status	Former	Former	1/2 PPD	N/A	1/2 PPD
Vitamin D Level	N/A	24.6	N/A	N/A	N/A

Table 7: Histologically Identified Sclerotic Bone							
Sample 111	Sample 119	Sample 130	Sample 131	Sample 133	Sample 152	Sample 157	Sample 180
+	+	+	+	+	+	+	+

Osteophytes

The articular surface of each sample was analyzed for cartilage loss. Areas where the cartilage was completely eroded, and the sclerotic bone was continuous with the surface, were identified as osteophytes. Six out of eight samples had an osteophyte (Table 9).

Sample 180

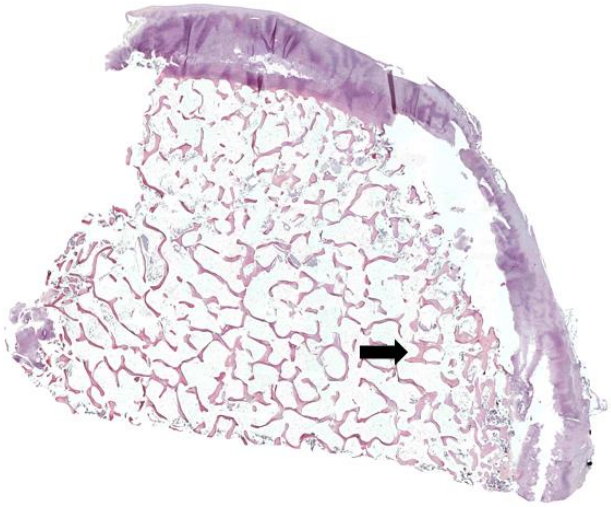

Sample 111

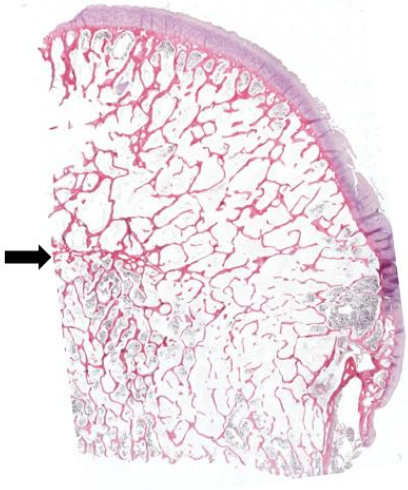

Sample 152

Sample 157

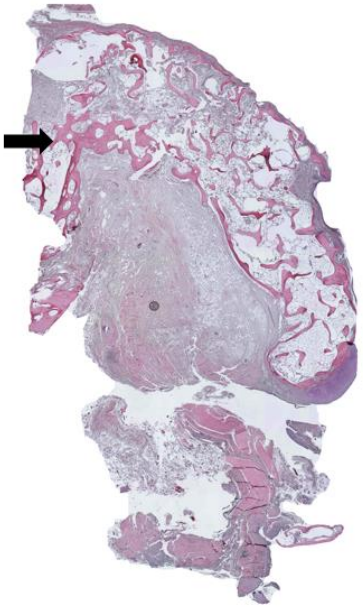

Figure 8: Sclerotic Bone. Four samples with arrows pointing to regions of sclerotic bone.

Table 8: Histologically Identified Subchondral Bone Cysts								
	Sample 111	Sample 119	Sample 130	Sample 131	Sample 133	Sample 152	Sample 157	Sample 180
Fibrous Cyst	-	+	+	+	-	+	+	-
Fatty Cyst	+	-	-	-	+	-	-	-
Cartilage Intrusion	-	+	-	-	-	-	-	-

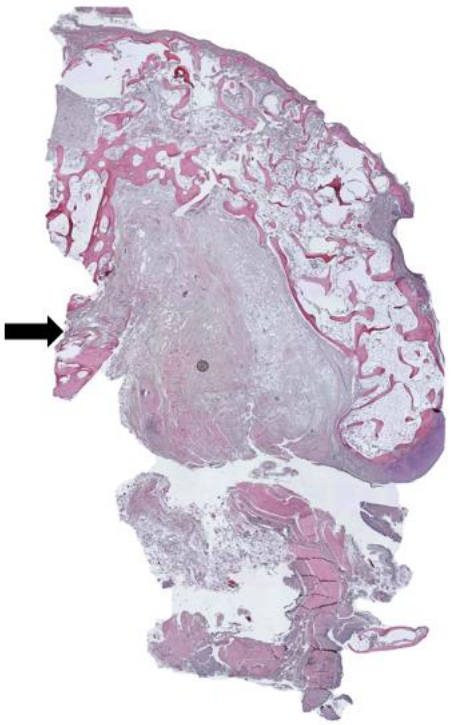

Figure 9: Fibrous Cyst. Arrow pointing to fibrous cyst region of Sample 157 stained with H&E

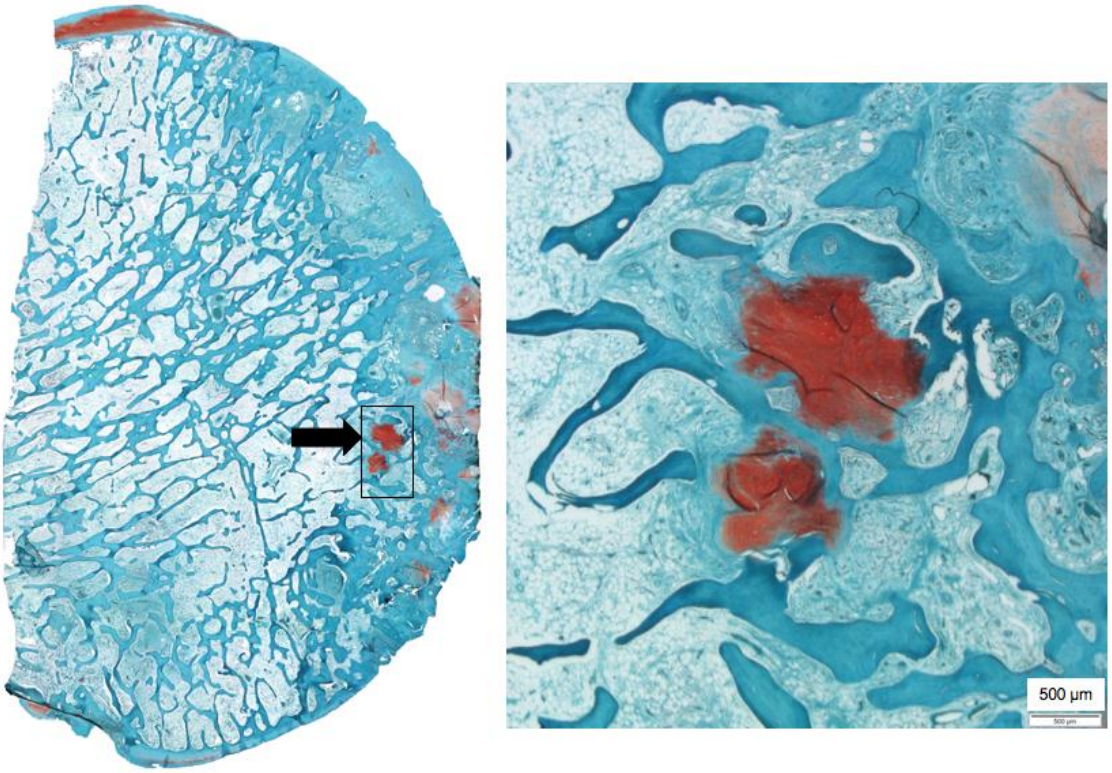

Figure 10: Cartilage Intrusion. Left: Arrow pointing to region of interest containing cartilage intrusion; Right: Region of interest magnified 4x

Table 9: Histologically Identified Osteophytes							
Sample 111	Sample 119	Sample 130	Sample 131	Sample 133	Sample 152	Sample 157	Sample 180
-	+	+	+	+	+	+	-

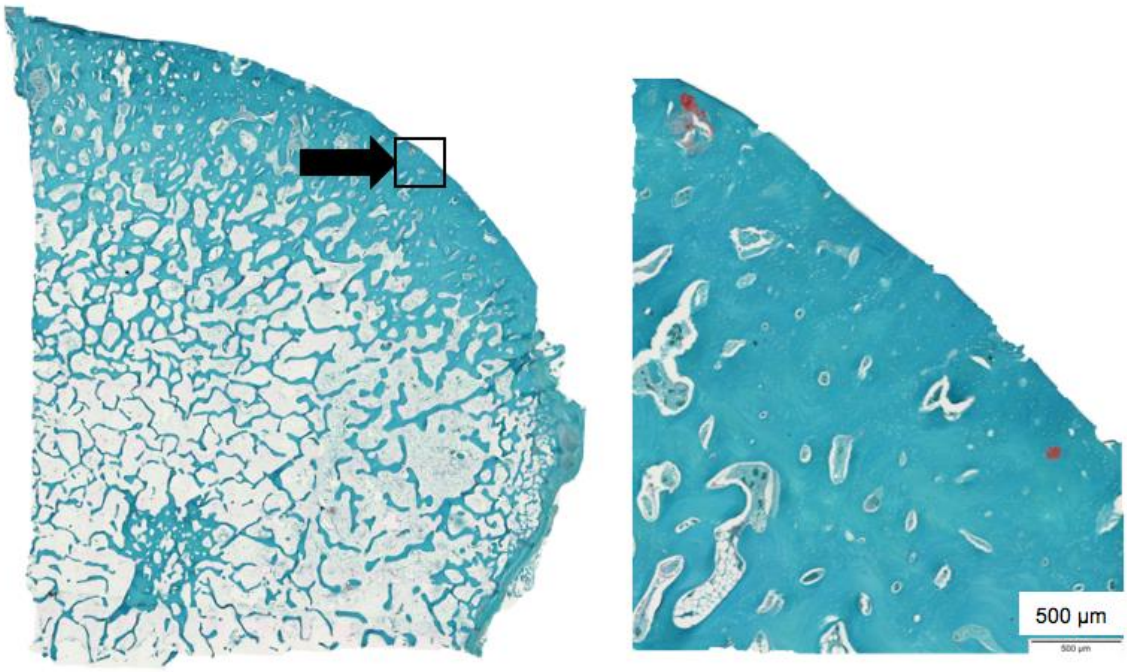

Figure 11: Osteophyte. Left: The blue sclerotic bone is continuous with the articular surface of this sample. Healthy cartilage would appear red when stained with Safarin-O/Fast Green. Arrow points to the region of interest; Right: Region of interest magnified 4x

Nerve Characteristics

Nerves were visualized with an antibody to PGP 9.5. Sample 133 was used to test different concentrations of the primary antibody, the effect of counterstaining with Hematoxylin, and the effect of using a heat retrieval method (Figures 12 and 13).

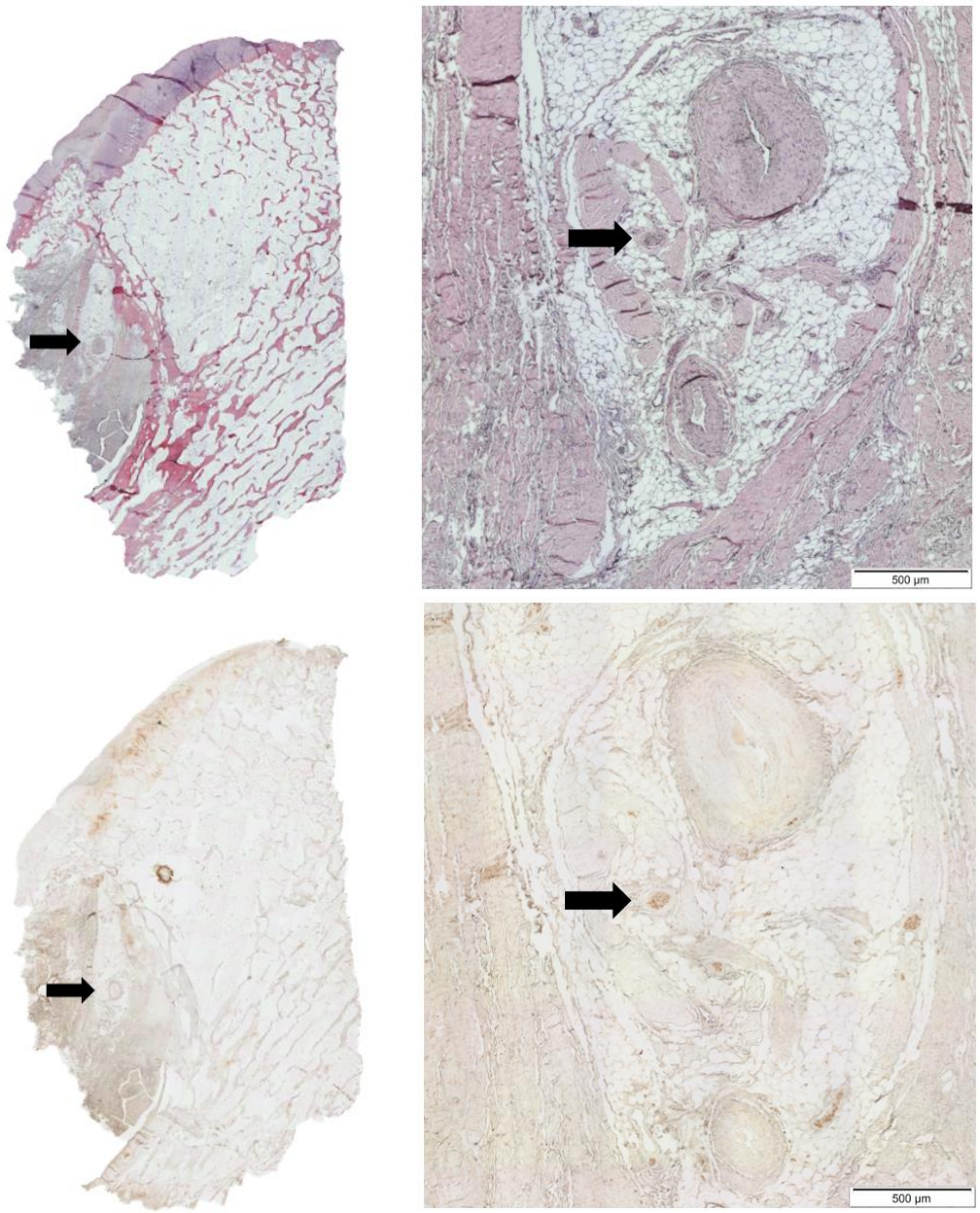

Figure 12: Sample 133 Region of Interest. Top Left: H&E with arrow pointing to region containing vessels and nerves; Top Right: H&E region of interest magnified 4x with arrow pointing to nerve; Bottom Left: PGP 9.5 without Hematoxylin, heat retrieval, or amplification, with arrow pointing to region containing vessels and nerves; Bottom Right: Region of interest magnified 4x stained with PGP 9.5 without Hematoxylin, heat retrieval, or amplification, with arrow pointing to nerve

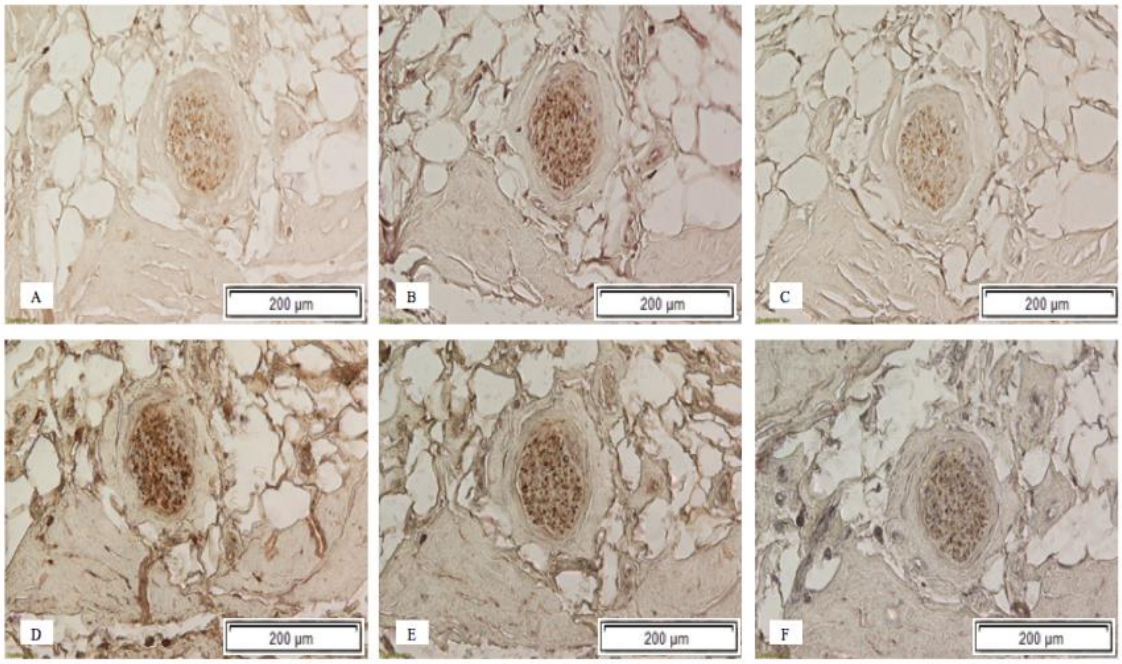

Figure 13: Sample 133 Nerve Magnified 20x. A: PGP 9.5 1:50 dilution counterstained with Hematoxylin; B: PGP 9.5 1:100 dilution counterstained with Hematoxylin; C: PGP 9.5 1:500 dilution counterstained with Hematoxylin; D: PGP 9.5 1:50 dilution counterstained with Hematoxylin and heat-retrieved; E: PGP 9.5 1:100 dilution counterstained with Hematoxylin and heat-retrieved; F: PGP 9.5 1:500 dilution counterstained with Hematoxylin and heat-retrieved

After performing this test, it was concluded that the optimal dilution was 1:100. Heat retrieval and Hematoxylin were removed from the protocol to attempt to reduce artefactual folding of the tissue (figure 14). The 1:100 dilution was then used to stain Sample 133, followed by amplification (figure 15).

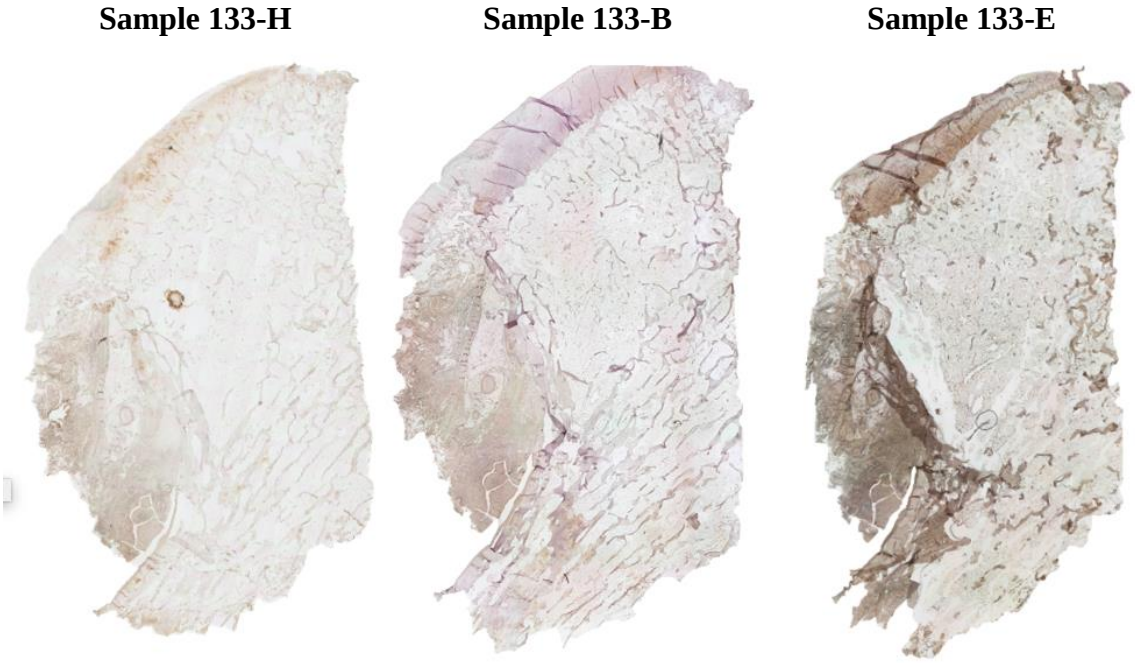

Figure 14: Artefactual folds in PGP 9.5-stained tissue. Left: Sample 133-H: PGP 9.5 1:100 dilution; Middle: Sample 133-B: PGP 9.5 1:100 dilution counterstained with Hematoxylin; Right: Sample 133-E: PGP 9.5 1:100 dilution counterstained with Hematoxylin and heat-retrieved

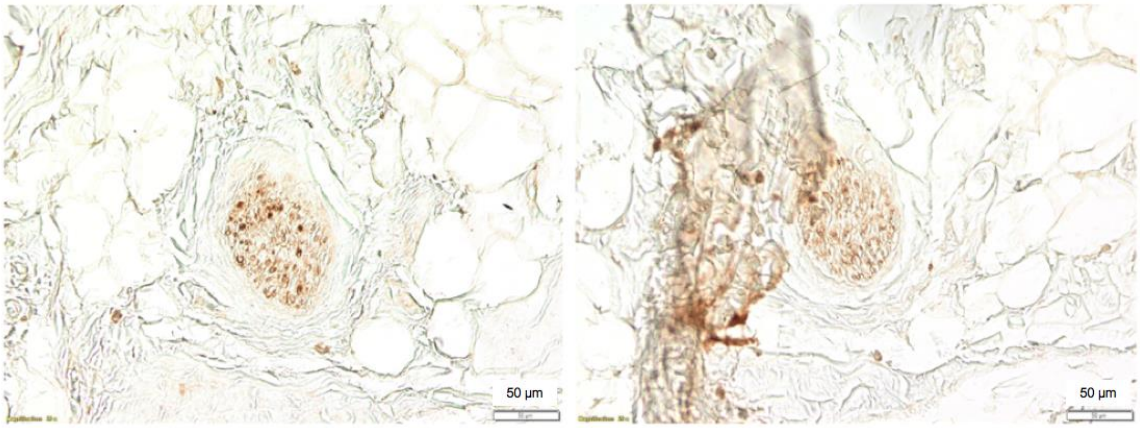

Figure 15: The effect of amplification on staining with PGP 9.5. Left: Sample 133-H: PGP 9.5 1:100 dilution magnified 20x; Right: Sample 133-G: PGP 9.5 1:100 dilution with amplification magnified 20x

After completing the experiments to evaluate the optimal staining conditions for PGP 9.5, all samples were stained and evaluated for PGP 9.5-positive nerves (Table 10). Special attention was paid to the cyst regions of samples that had fibrous subchondral bone cysts because these are the most likely type to undergo neurovascular invasion (Table 11).

Table 10: PGP 9.5-Positive Nerves

Sample 111	Sample 119	Sample 130	Sample 131	Sample 133	Sample 152	Sample 157	Sample 180
+	-	+	+	+	-	+	-

Table 11: PGP 9.5-Positive Nerves Within Fibrous Subchondral Bone Cysts

Sample 119	Sample 130	Sample 131	Sample 152	Sample 157
-	+	+	-	+

In each sample containing a PGP 9.5-positive nerve, the nerve was close to a muscular artery. In Sample 111, the nerve was located close to the border between the femoral head and neck (Figure 16). Sample 130 had a nerve in the fibrous cyst region (Figure 17). The nerve was surrounded by several muscular arteries and dense irregular connective tissue. Sample 131 had nerves in both cyst and non-cyst regions, but a nerve from the non-cyst region was chosen for Figure 18 because the cyst region of this sample was not well preserved. Sample 157 had a nerve in the fibrous cyst region (Figure 19). This sample was in PFA for only one week prior to decalcification, with the goal of comparing the staining properties of the nerves in this sample to those of samples fixed for two weeks. Qualitatively, the nerve in Sample 157 does not appear to have had better

binding to the PGP 9.5 antibody; it is not darker than its counterparts in the other samples. Sample 157 also did not appear to have a greater frequency of stained nerves than the other samples.

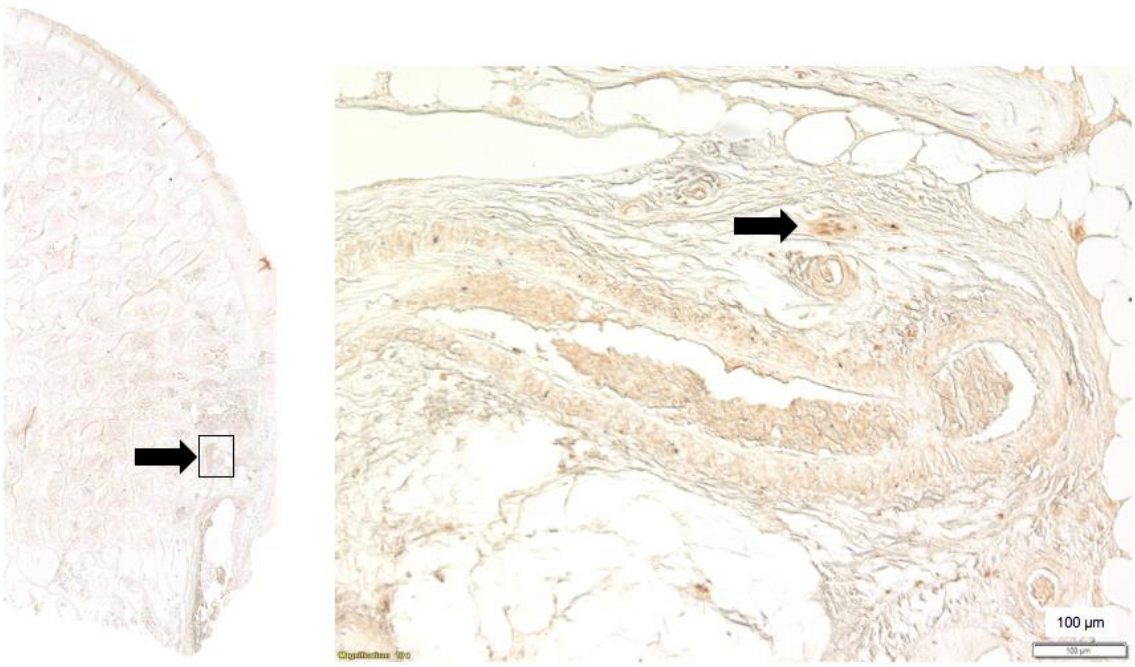

Figure 16: PGP 9.5-Positive Nerve in a Non-Cyst Region of Sample 111. Left: Overview image of Sample 111 with arrow pointing to region of interest containing nerve; Right: Region of interest with arrow pointing to PGP 9.5-positive nerve magnified 10x

Figure 17: PGP 9.5-Positive Nerve in Fibrous Cyst Region of Sample 130. Left: Overview image of Sample 130 with arrow pointing to region of interest containing nerve; Right: Region of interest magnified 10x

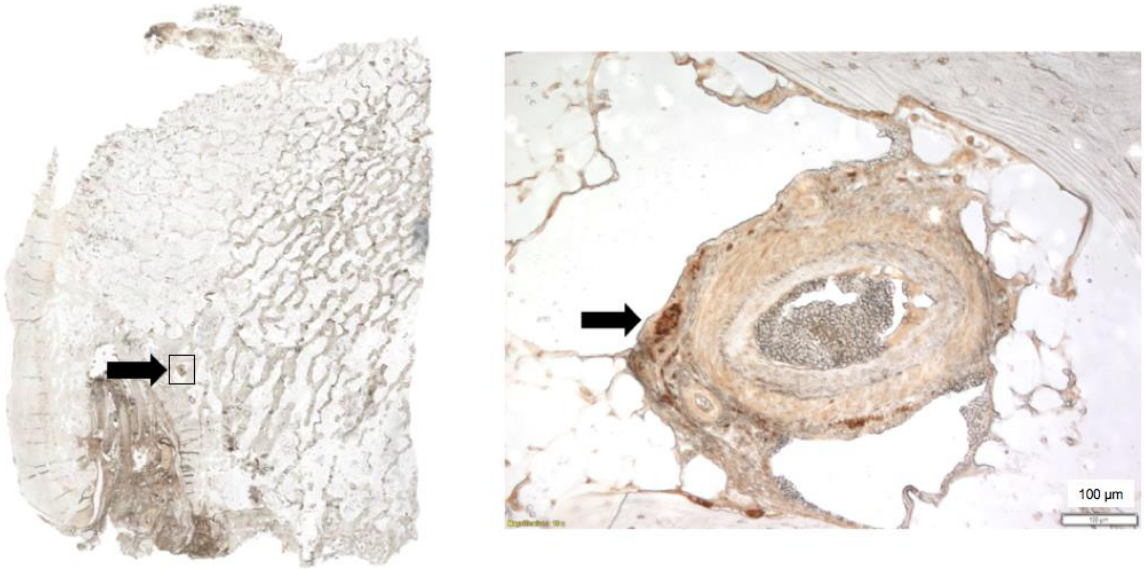

Figure 18: PGP 9.5-Positive Nerve in a Non-Cyst Region of Sample 131. Left: Overview image of Sample 131 with arrow pointing to region of interest containing nerve; Right: Region of interest magnified 10x with arrow pointing to PGP 9.5-positive nerve

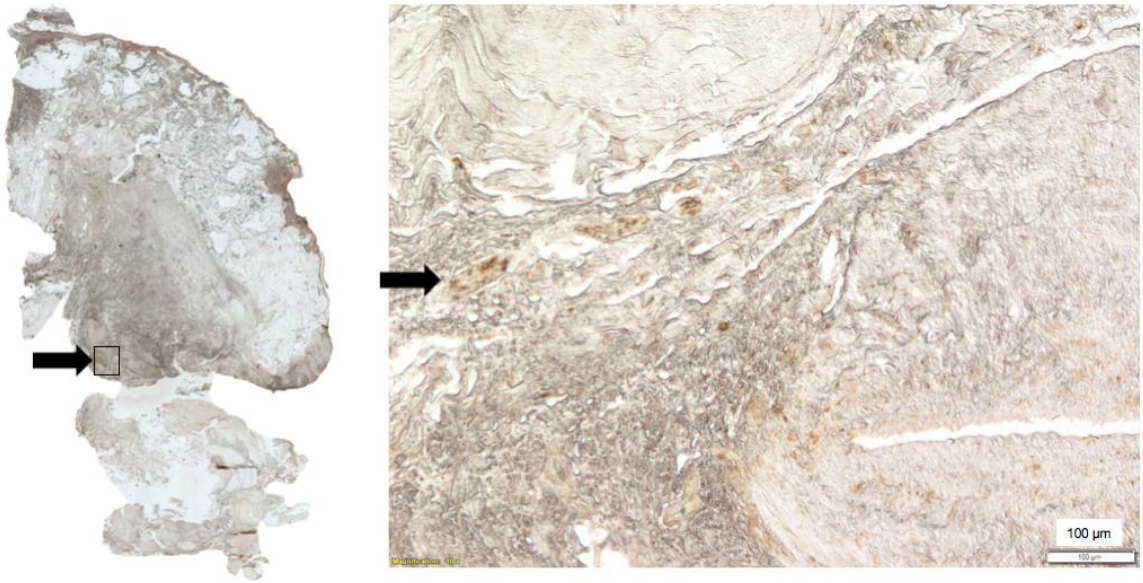

Figure 19: PGP 9.5-Positive Nerve in Fibrous Cyst Region of Sample 157. Left: Overview image of Sample 157 with arrow pointing to region of interest containing nerve; Right: Region of interest magnified 10x with arrow pointing to leftmost portion of PGP 9.5-positive nerve. The nerve runs longitudinally relative to the muscular artery near it

Blood Vessel Characteristics

Blood vessels were visualized with an antibody to CD31. Sample 119 was identified to have blood vessels present in H&E, and was therefore used to test different staining conditions (Figure 20).

Sample 119-A

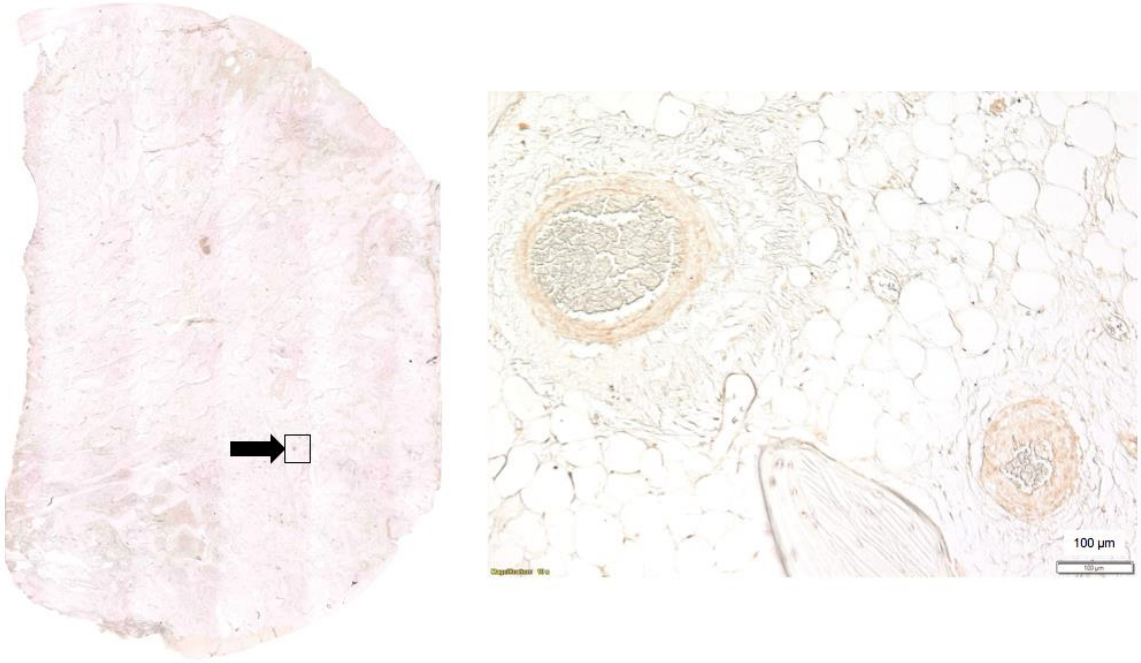

Sample 119-B

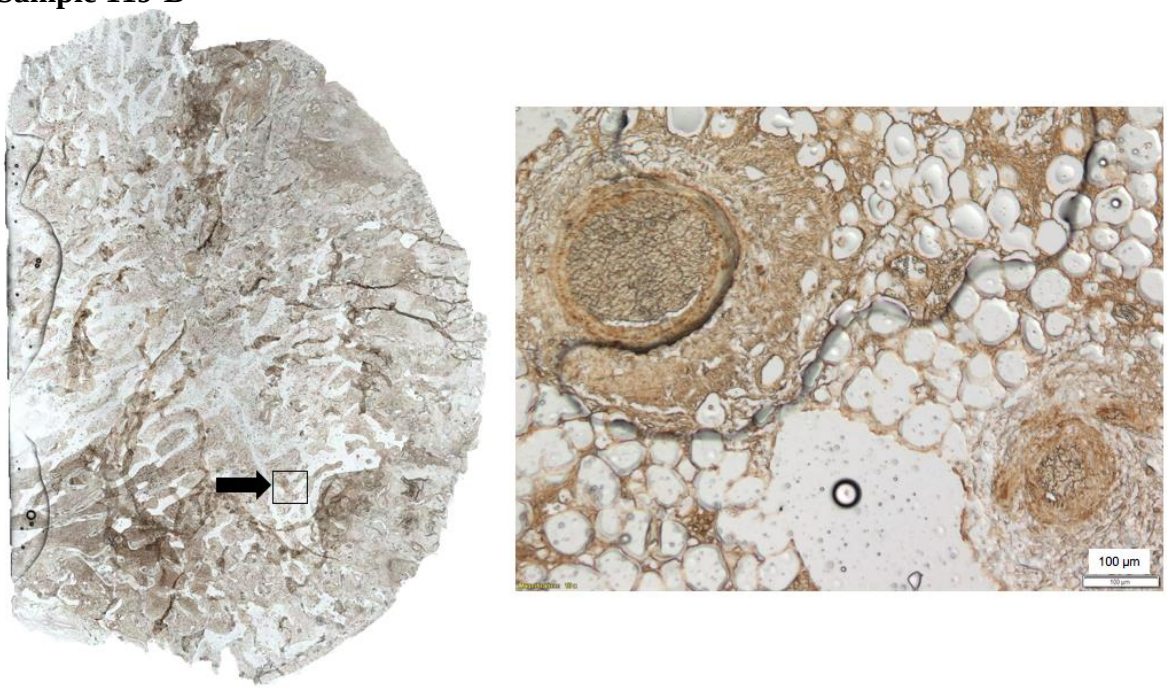

Figure 20: Blood vessels stained with CD31 with and without heat retrieval. Top left: overview of Sample 119 stained without heat retrieval. Top right: CD31-marked blood vessels magnified 10x. Bottom left: overview of Sample 119 stained with heat retrieval. Bottom right: CD31-marked blood vessels magnified 10x

As with PGP 9.5, samples that were heat-retrieved and stained with CD31 had more artefactual folds than samples that were not heat-retrieved. The folds in some cases completely obscured the blood vessels. It was concluded that heat-retrieval was not necessary for visualizing vessels.

Samples stored in PFA for varying amounts of time were used to evaluate the effect of time spent in PFA on clarity of antibody stain. Sample 152 was fixed in PFA for two weeks prior to decalcification, and was found to have a CD31-positive arteriole (Figure 21). The arteriole found in Sample 152, compared to blood vessels in Samples 157 and 180, which were fixed for one week and zero weeks respectively, qualitatively appears to have the same ability to bind the CD31 antibody. Sample 180 had fewer blood vessels than Samples 152 and 157, and did not have any CD31-positive muscular arteries. An arteriole from Sample 180 is shown in Figure 22. Figure 23 shows several arterioles and a muscular artery in Sample 157.

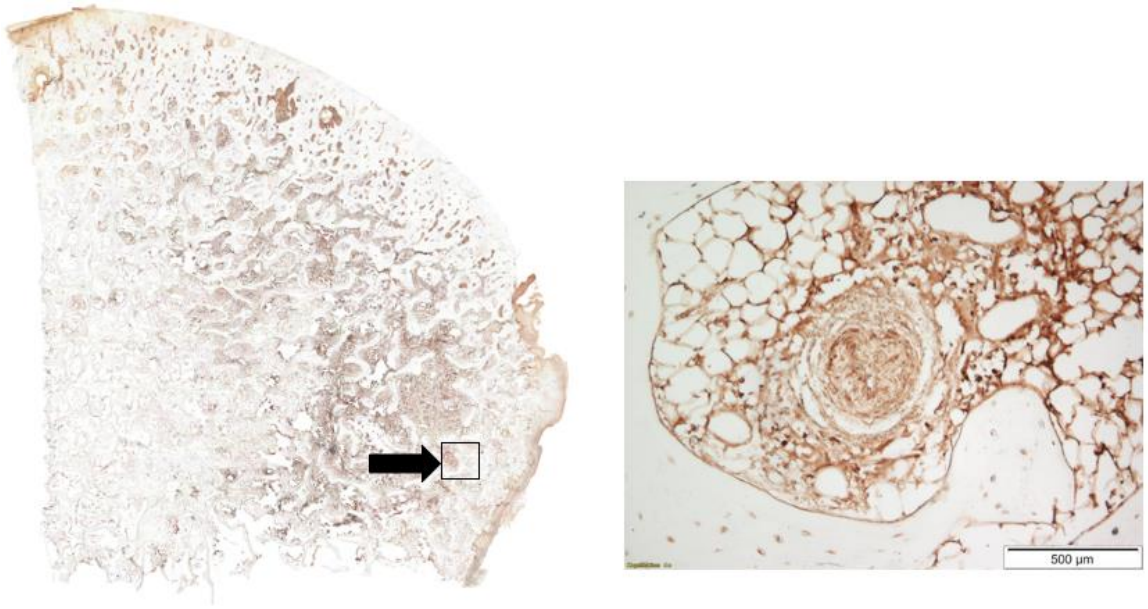

Figure 21: CD31-Positive Blood Vessel in Cyst Region of Sample 152. Left: Overall image of Sample 152 stained with CD31 with arrow pointing to region of interest; Right: CD31-positive arteriole within the region of interest magnified 4x

Figure 22: CD31-Positive Blood Vessel in a Non-Cyst Region of Sample 180. Left: Overall image of Sample 180 stained with CD31 with arrow pointing to region of interest; Right: Blood vessel positive for CD31 magnified 4x

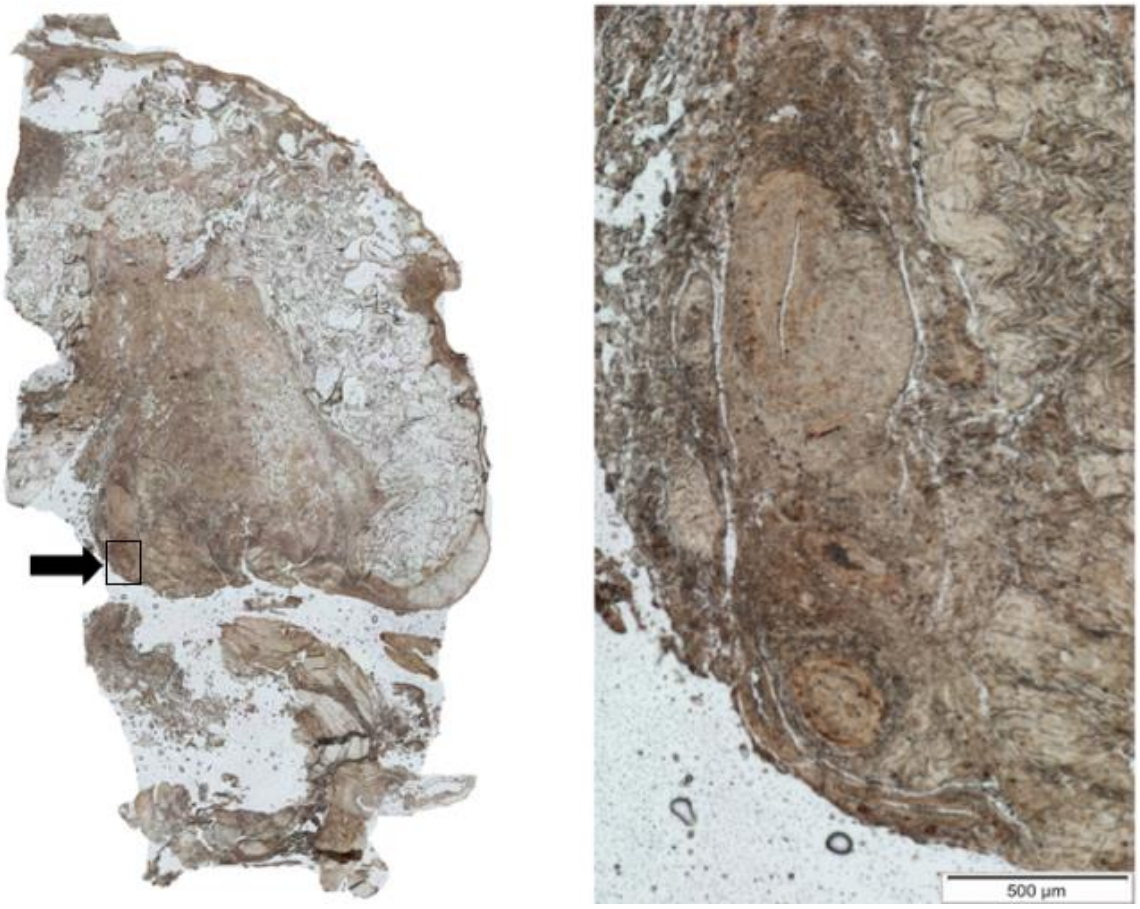

Figure 23: CD31-Positive Blood Vessels in Fibrous Cyst Region of Sample 157. Left: Overall image of Sample 157 stained with CD31 with arrow pointing to region of interest within the fibrous subchondral cyst; Right: Within the region of interest, several CD31-positive blood vessels can be seen at 4x magnification

After completing the experiments to evaluate the optimal staining conditions for CD31, all samples were stained and evaluated for CD31-positive vessels (Table 12). Special attention was paid to the cyst regions of samples that had fibrous subchondral

bone cysts (Table 13). All samples were found to have CD31-positive vessels. A cluster of vessels typical of those found in fibrous cyst regions is shown in figure 24.

Table 12: CD31-Positive Blood Vessels

Sample 111	Sample 119	Sample 130	Sample 131	Sample 133	Sample 152	Sample 157	Sample 180
+	+	+	+	+	+	+	+

Table 13: CD31-Positive Blood Vessels Within Fibrous Subchondral Bone Cysts

Sample 119	Sample 130	Sample 131	Sample 152	Sample 157
+	+	+	+	+

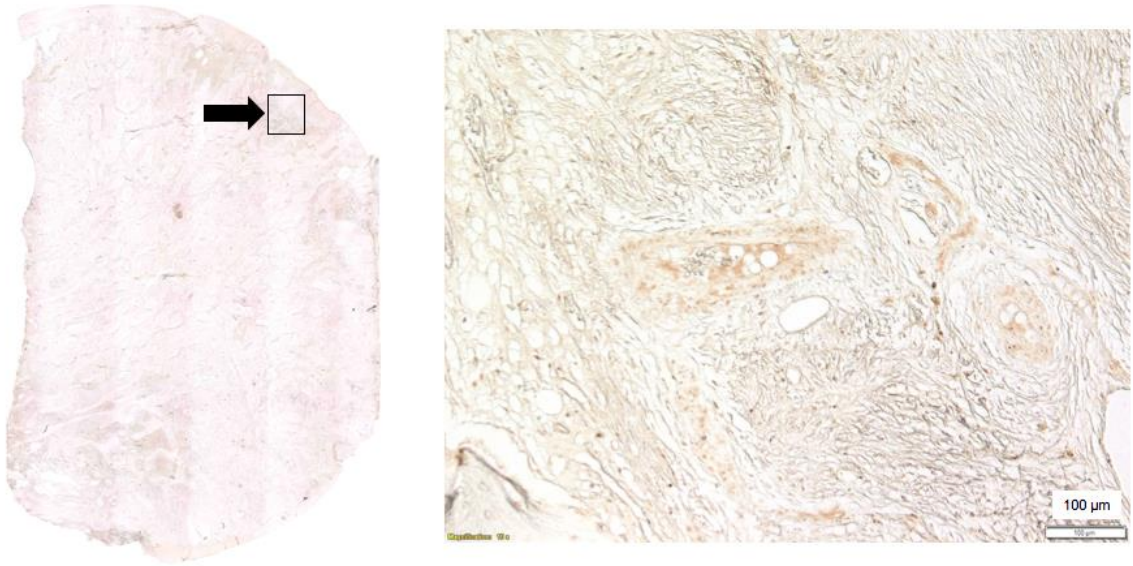

Figure 24: CD31-Positive Blood Vessels in Cyst Region of Sample 119. Left: Overall image of Sample 119 stained with CD31 with arrow pointing to region of interest within fibrous subchondral bone cyst; Right: Blood vessels positive for CD31 magnified 10x

DISCUSSION

OA affects the whole hip joint, and causes pathological subchondral bone remodeling resulting in subchondral bone cysts, osteophytes, and cartilage loss. With this remodeling, an increased number of blood vessels was expected and has been observed in human samples (Shabestari et al. 2016). Nerves are known to be associated with vessels, therefore an increase in the number of peripheral nerves in OA bone was expected, although it had not been previously demonstrated in subchondral bone of osteoarthritic femoral heads. In this study, a reproducible histological technique to identify blood vessels and nerve in bone sections was created and applied to osteoarthritic femoral heads. Analysis of sclerotic bone, subchondral bone cysts, and osteophytes was done to establish the environment of the regions in which blood vessels and nerves were found.

Histological Technique

The immunochemistry techniques designated as optimal were selected to maximize signal intensity from target tissues while minimizing tissue folding and background signal. For both anti-CD31 and anti-PGP 9.5, a 1:100 dilution and amplification were optimal. In future, heat-retrieval may work well for increasing signal intensity in samples that do not stain well with amplification and without heat-retrieval. Counterstaining with Hematoxylin, which was also found to increase tissue folding, may be used if basophilic structures need to be identified. In this study, use of samples stained

with Safarin-O/Fast Green allowed visualization of cartilage, so it was not as necessary to counterstain immunohistochemistry slides with Hematoxylin.

The effect of fixation time on the staining properties of nerves in osteoarthritic marrow regions of the femoral head was unable to be determined due to the lack of visible nerves in Sample 152 and Sample 180. Sample 157, which was only fixed for one week before decalcification, had PGP 9.5 positive nerves, but the number and image quality was not qualitatively different from the samples with a longer fixation period.

Both CD31 and PGP 9.5 stained tissues that were clearly not blood vessel endothelium and nerve, respectively. Red blood cells were frequently observed to be stained. When identifying nerves, the possibility of artefactual staining of non-target tissue was taken into account to avoid falsely identifying blood-filled veins and venules as nerves. Location was a useful indicator. For example, sometimes a structure would appear to be a nerve, but if it was followed through the tissue it was actually continuous with a vessel. Osteoblasts were also observed to be positive for PGP 9.5, but the cuboidal morphology of these cells is dissimilar to the structure of peripheral nerves, so it was not difficult to correctly identify them as osteoblasts. In many cases, reference to the corresponding slide stained with H&E was also useful for determining the identity of structures stained with PGP 9.5.

Blood Vessel and Nerve Characteristics Within Osteoarthritic Femoral Heads

All eight samples were found to have sclerotic bone. The sclerotic bone was used to identify subchondral bone cysts. Since all samples were from subjects with late stage

OA, this was an anticipated result. Six out of eight samples were found to have osteophytes.

Seven out of eight samples were found to have subchrondral bone cysts upon histological analysis. Sample 180 did not have an identifiable cyst region on μCT, and correspondingly did not have a histologically identified subchondral bone cyst.

All eight samples had CD31-positive blood vessels. All five samples with fibrous subchondral bone cysts had CD31-positive blood vessels in the cyst region. In future, the anti-CD31 stain can be used to quantify the number of blood vessels in each sample, and compare the blood vessel characteristics of different types of cysts.

PGP 9.5-positive nerves were found in five out of eight samples. Three out of five samples containing fibrous subchondral bone cysts had PGP 9.5-positive nerves in the cyst region. All nerves identified were close to a muscular artery. In future, the anti-PGP 9.5 stain can be used to compare the location and quantity of nerves in different types of cysts.

The articular cartilage of Sample 130 superficial to the nerve was not well preserved, but it was concluded that fibrous tissue near where the articular cartilage represented a cyst region. This fibrous tissue contained nerves and vessels, but due to the damage in the surrounding region, images of these structures were not included.

In future, a larger sample set will be used to correlate the nature of blood vessel density and nerves that are found in bone marrow lesions identified on MRI scans obtained before surgery and are associated with bone cysts. Quantification of nerve and blood vessel characteristics has not been performed prior to this study. Comparison of

these structures within different types of subchondral bone cysts will show which tissue composition is most likely to have pathological blood vessel and nerve growth. For example, in this study most of the samples had fibrous cysts, but with a larger sample size there will be more cartilage intrusions to compare. With this larger sample size, it will be possible to tell whether fibrous cysts or cartilage intrusions have more blood vessels and nerves. Comparison will also be made between cysts of different size and location relative to the articular surface. This level of specific analysis of subchondral bone cysts has not yet been described in the literature. If nerve is found in subchondral bone cysts, the cause of pain associated with hip OA will be elucidated. This is an important step towards identifying more effective treatments for OA that address the specific underlying causes and the development of non-treatable pain.

Limitations

This study had several limitations. Ideally, when sectioning samples using the Isomet 4000, coronal slices should be obtained to keep the plane of section constant between samples and constant with previous studies done. Coronal slices could not be obtained because the clamp holding the sample in place on the Isomet 4000 was not large enough. Additionally, to aid in dissecting out cysts, a cyst overlay should be used to visualize cyst position relative to the cutting plane.

The small sample size of this study was a limitation with regard to identifying blood vessel and nerve characteristics within osteoarthritic femoral heads. This limitation

will be overcome in the next study, where 50 samples will be processed according to the procedure developed here.

CONCLUSION

All eight samples had CD31-positive blood vessels. All five samples with fibrous subchondral bone cysts had CD31-positive blood vessels in the cyst region. If BMLs accurately represent histological cyst regions, then his result agrees with the finding of Shabestari et al. in 2016 that MRI-identified BMLs had CD31-positive vessels (Shabestari et al. 2016). The antibody to CD31 worked best under the conditions of no heat-retrieval or Hematoxylin-counterstain. Fixation time did not have an effect on staining with CD31.

PGP 9.5-positive nerves were found in five out of eight samples. Three out of five samples containing fibrous subchondral bone cysts had PGP 9.5-positive nerves in the cyst region. All nerves identified were close to a muscular artery. This result is consistent with the finding of Netzer et al. in 2016 that PGP 9.5-positive nerves in bone from subjects with lumbar spinal stenosis were associated with arteries (Netzer et al. 2016). The antibody to PGP 9.5 worked best under the conditions of no heat-retrieval or Hematoxylin-counterstain.

Developing reproducible procedures for staining with anti-CD31 and anti-PGP 9.5 is an important step in protocol development. The next study will use these procedures to identify blood vessels and nerves so that these structures can be accurately compared with MRI-identified BMLs.

The association between subchondral bone cysts and pain has been studied in hip OA, but the exact histological nature of MRI lesions to structural loss and tissue composition has not been well defined. Subjects with OA-associated bone cysts were found to have more pain than subjects without bone cysts (Kumar et al. 2013). If subchondral bone cysts were identified to be correlated with MRI-identified BMLs, then it could be concluded that BMLs are associated with structures known to cause pain. This would be a useful tool in the clinic for identifying when and how to treat osteoarthritic pain.

REFERENCES

Altman, R., Alarcón, G., Appelrouth, D., Bloch, D., Borenstein, D., Brandt, K., Brown, C., Cooke, T. D., Daniel, W., Feldman, D., Greenwald, R., Hochberg, M., Howell, D., Ike, R., Kapila, P., Kaplan, D., Koopman, W., Marino, C., McDonald, E., McShane, D. J., Medsger, T., Michel, B., Murphy, W. A., Osial, T., Ramsey-Goldman, R., Rothschild, B. and Wolfe, F. (1991), The American College of Rheumatology criteria for the classification and reporting of osteoarthritis of the hip. *Arthritis & Rheumatism*, 34: 505–514. doi:10.1002/art.1780340502

Aigner, T, and Stove, J. 2003. "Collagens—major Component of the Physiological Cartilage Matrix, Major Target of Cartilage Degeneration, Major Tool in Cartilage Repair." *Advanced Drug Delivery Reviews* 55 (12): 1569–93. https://doi.org/10.1016/j.addr.2003.08.009.

Barrett, Kim E., Susan M. Barman, Scott Boitano, and Heddwen L. Brooks. 2016. "Hormonal Control of Calcium & Phosphate Metabolism & the Physiology of Bone." In *Ganong's Review of Medical Physiology, 25e*. New York, NY: McGraw-Hill Education. accessmedicine.mhmedical.com/content.aspx?aid=1115830339.

Chen, Y., T. Wang, M. Guan, W. Zhao, F.-K.-L. Leung, H. Pan, X. Cao, X.E. Guo, and W.W. Lu. 2015. "Bone Turnover and Articular Cartilage Differences Localized to Subchondral Cysts in Knees with Advanced Osteoarthritis." *Osteoarthritis and Cartilage* 23 (12): 2174–83. https://doi.org/10.1016/j.joca.2015.07.012.

Cher, Jonathon Z.B., Moeed Akbar, Susan Kitson, Lindsay A.N. Crowe, Emma Garcia-Melchor, Stephen C. Hannah, Michael McLean, et al. 2017. "Alarmins in Frozen Shoulder: A Molecular Association Between Inflammation and Pain." *The American Journal of Sports Medicine*, November, 36354651774112. https://doi.org/10.1177/0363546517741127.

Cross, Marita, Emma Smith, Damian Hoy, Sandra Nolte, Ilana Ackerman, Marlene Fransen, Lisa Bridgett, et al. 2014. "The Global Burden of Hip and Knee Osteoarthritis: Estimates from the Global Burden of Disease 2010 Study." *Annals of the Rheumatic Diseases* 73 (7): 1323–30. https://doi.org/10.1136/annrheumdis-2013-204763.

Drake, Richard L., Wayne A. Vogl, and Adam W. M. Mitchell. 2012. *Gray's Basic Anatomy: Study Smart with Student Consult*. Philadelphia, PA: Elsevier, Churchill Livingstone.

Feeko, Kristofer J., and Michael Mallow. 2015. "Kinesiology." In *CURRENT Diagnosis & Treatment: Physical Medicine & Rehabilitation*, edited by Ian B. Maitin and

Ernesto Cruz. New York, NY: McGraw-Hill Education. accessmedicine.mhmedical.com/content.aspx?aid=1105126775.

Felson, David T. 2015. "Osteoarthritis." In *Harrison's Principles of Internal Medicine, 19e*, edited by Dennis Kasper, Anthony Fauci, Stephen Hauser, Dan Longo, J. Larry Jameson, and Joseph Loscalzo. New York, NY: McGraw-Hill Education. accessmedicine.mhmedical.com/content.aspx?aid=1120814183.

Gamble, Roche, Johnson Wyeth-Ayerst, Eli Lilly Johnson, Wyeth-Ayerst Searle, and S. Beecham. 2000. "Recommendations for the Medical Management of Osteoarthritis of the Hip and Knee." *Arthritis & Rheumatism* 43 (9): 1905–1915.

Glyn-Jones, Sion, A. J. R. Palmer, A. J. Price, T. L. Vincent, Harrie Weinans, and Andrew Jonathan Carr. 2015. "Osteoarthritis." *The Lancet* 386 (9991): 376–387.

Gray, Henry. 1918. *Anatomy of the Human Body*. 20th ed. Philadelphia, PA: Lea & Febiger. http://www.bartleby.com/107/illus247.html.

Hellmann, David B., and John B. Imboden Jr. 2017. "Rheumatologic, Immunologic, & Allergic Disorders." In *Current Medical Diagnosis & Treatment 2018*, edited by Maxine A. Papadakis, Stephen J. McPhee, and Michael W. Rabow. New York, NY: McGraw-Hill Education. accessmedicine.mhmedical.com/content.aspx?aid=1145403555.

Hügle, Thomas, and Jeroen Geurts. 2016. "What Drives Osteoarthritis?—synovial *versus* Subchondral Bone Pathology." *Rheumatology*, December, kew389. https://doi.org/10.1093/rheumatology/kew389.

Ip, David. 2005. *Orthopedic Principles: A Resident's Guide*. Berlin: Springer.

Jordan, Joanne M., Charles G. Helmick, Jordan B. Renner, Gheorghe Luta, Anca D. Dragomir, Janice Woodard, Fang Fang, Todd A. Schwartz, Amanda E. Nelson, and Lauren M. Abbate. 2009. "Prevalence of Hip Symptoms and Radiographic and Symptomatic Hip Osteoarthritis in African Americans and Caucasians: The Johnston County Osteoarthritis Project." *The Journal of Rheumatology* 36 (4): 809–815.

Klose-Jensen, R., L.B. Hartlev, L.W.T. Boel, M.B. Laursen, K. Stengaard-Pedersen, K.K. Keller, and E.-M. Hauge. 2015. "Subchondral Bone Turnover, but Not Bone Volume, Is Increased in Early Stage Osteoarthritic Lesions in the Human Hip Joint." *Osteoarthritis and Cartilage* 23 (12): 2167–73. https://doi.org/10.1016/j.joca.2015.06.001.

Kumar, D., C.R. Wyatt, S. Lee, L. Nardo, T.M. Link, S. Majumdar, and R.B. Souza. 2013. “Association of Cartilage Defects, and Other MRI Findings with Pain and Function in Individuals with Mild–moderate Radiographic Hip Osteoarthritis and Controls.” *Osteoarthritis and Cartilage* 21 (11): 1685–92. https://doi.org/10.1016/j.joca.2013.08.009.

Kurtz, Steven. 2007. “Projections of Primary and Revision Hip and Knee Arthroplasty in the United States from 2005 to 2030.” *The Journal of Bone and Joint Surgery (American)* 89 (4): 780. https://doi.org/10.2106/JBJS.F.00222.

Lafage-Proust, Marie-Hélène, Bernard Roche, Max Langer, Damien Cleret, Arnaud Vanden Bossche, Thomas Olivier, and Laurence Vico. 2015. “Assessment of Bone Vascularization and Its Role in Bone Remodeling.” *BoneKEy Reports* 4 (April). https://doi.org/10.1038/bonekey.2015.29.

Landells, J. W. 1953. “The Bone Cysts of Osteoarthritis.” *Bone & Joint Journal* 35 (4): 643–649.

Li, Guangyi, Qiujian Zheng, Euphemie Landao-Bassonga, Tak S. Cheng, Nathan J. Pavlos, Yuanchen Ma, Changqing Zhang, and Ming H. Zheng. 2015. “Influence of Age and Gender on Microarchitecture and Bone Remodeling in Subchondral Bone of the Osteoarthritic Femoral Head.” *Bone* 77 (August): 91–97. https://doi.org/10.1016/j.bone.2015.04.019.

Mescher, Anthony L. 2013. “Chapter 7. Cartilage.” In *Junqueira’s Basic Histology, 13e*. New York, NY: The McGraw-Hill Companies. accessmedicine.mhmedical.com/content.aspx?aid=57331104.

———. 2016. “Bone.” In *Junqueira’s Basic Histology, 14e*. New York, NY: McGraw-Hill Education. accessmedicine.mhmedical.com/content.aspx?aid=1133855761.

Neogi, Tuhina, and Yuqing Zhang. 2013. “Epidemiology of Osteoarthritis.” *Rheumatic Disease Clinics of North America* 39 (1): 1–19. https://doi.org/10.1016/j.rdc.2012.10.004.

Netzer, Cordula, Karin Urech, Thomas Hügle, Robyn Melanie Benz, Jeroen Geurts, and Stefan Schären. 2016. “Characterization of Subchondral Bone Histopathology of Facet Joint Osteoarthritis in Lumbar Spinal Stenosis: FACET JOINT OSTEOARTHRITIS IN SPINAL STENOSIS.” *Journal of Orthopaedic Research* 34 (8): 1475–80. https://doi.org/10.1002/jor.23281.

Pivec, Robert, Aaron J. Johnson, Simon C. Mears, and Michael A. Mont. 2012. “Hip Arthroplasty.” *The Lancet* 380 (9855): 1768–1777.

Roach, H, and Tilley, S. 2007. “The Pathogenesis of Osteoarthritis.” In *Bone and Osteoarthritis*, edited by Felix Bronner and Mary C. Farach-Carson, 1–18. V.4. London: Springer.

Roemer, F.W., R. Frobell, D.J. Hunter, M.D. Crema, W. Fischer, K. Bohndorf, and A. Guermazi. 2009. “MRI-Detected Subchondral Bone Marrow Signal Alterations of the Knee Joint: Terminology, Imaging Appearance, Relevance and Radiological Differential Diagnosis.” *Osteoarthritis and Cartilage* 17 (9): 1115–31. https://doi.org/10.1016/j.joca.2009.03.012.

Saito, M., T. Sasho, S. Yamaguchi, N. Ikegawa, R. Akagi, Y. Muramatsu, S. Mukoyama, et al. 2012. “Angiogenic Activity of Subchondral Bone during the Progression of Osteoarthritis in a Rabbit Anterior Cruciate Ligament Transection Model.” *Osteoarthritis and Cartilage* 20 (12): 1574–82. https://doi.org/10.1016/j.joca.2012.08.023.

Shabestari, M., J. Vik, J.E. Reseland, and E.F. Eriksen. 2016. “Bone Marrow Lesions in Hip Osteoarthritis Are Characterized by Increased Bone Turnover and Enhanced Angiogenesis.” *Osteoarthritis and Cartilage* 24 (10): 1745–52. https://doi.org/10.1016/j.joca.2016.05.009.

Suri, S., S. E Gill, S. Massena de Camin, D. F McWilliams, D. Wilson, and D. A Walsh. 2007. “Neurovascular Invasion at the Osteochondral Junction and in Osteophytes in Osteoarthritis.” *Annals of the Rheumatic Diseases* 66 (11): 1423–28. https://doi.org/10.1136/ard.2006.063354.

Suri, Sunita, and David A. Walsh. 2012. “Osteochondral Alterations in Osteoarthritis.” *Bone* 51 (2): 204–11. https://doi.org/10.1016/j.bone.2011.10.010.

Tak, Erwin, Patricia Staats, Ariëtte Van Hespen, and Marijke Hopman-Rock. 2005. “The Effects of an Exercise Program for Older Adults with Osteoarthritis of the Hip.” *The Journal of Rheumatology* 32 (6): 1106–1113.

CURRICULUM VITAE